



Deposited via The University of Leeds.

White Rose Research Online URL for this paper:

<https://eprints.whiterose.ac.uk/id/eprint/175638/>

Version: Accepted Version

Article:

Wang, R, Yang, Y, Jing, Y et al. (2021) Molecular mechanisms of mutualistic and antagonistic interactions in a plant–pollinator association. *Nature Ecology & Evolution*, 5 (7). pp. 974-986. ISSN: 2397-334X

<https://doi.org/10.1038/s41559-021-01469-1>

© The Author(s), under exclusive licence to Springer Nature Limited 2021. This is an author produced version of an article published in *Nature Ecology and Evolution*. Uploaded in accordance with the publisher's self-archiving policy.

Reuse

Items deposited in White Rose Research Online are protected by copyright, with all rights reserved unless indicated otherwise. They may be downloaded and/or printed for private study, or other acts as permitted by national copyright laws. The publisher or other rights holders may allow further reproduction and re-use of the full text version. This is indicated by the licence information on the White Rose Research Online record for the item.

Takedown

If you consider content in White Rose Research Online to be in breach of UK law, please notify us by emailing eprints@whiterose.ac.uk including the URL of the record and the reason for the withdrawal request.

1 Molecular mechanisms of mutualistic and antagonistic interactions in a
2 plant-pollinator association

3 Rong Wang^{1,20†}, Yang Yang^{1†}, Yi Jing^{2†}, Simon T. Segar^{3†}, Yu Zhang¹, Gang Wang⁴,
4 Jin Chen⁴, Qing-Feng Liu², Shan Chen¹, Yan Chen⁵, Astrid Cruaud⁶, Yuan-Yuan
5 Ding¹, Derek W. Dunn⁷, Qiang Gao², Philip M. Gilmartin⁸, Kai Jiang¹, Finn
6 Kjellberg⁹, Hong-Qing Li¹⁰, Yuan-Yuan Li¹, Jian-Quan Liu¹¹, Min Liu¹², Carlos A.
7 Machado¹³, Ray Ming¹⁴, Jean-Yves Rasplus⁶, Xin Tong¹, Ping Wen⁴, Huan-Ming
8 Yang², Jing-Jun Yang¹, Ye Yin², Xing-Tan Zhang¹⁵, Yuan-Ye Zhang¹⁶, Hui Yu^{17,18*},
9 Zhen Yue^{2*}, Stephen G. Compton^{19*}, Xiao-Yong Chen^{1,20*}

10

11 ¹Zhejiang Tiantong Forest Ecosystem National Observation and Research Station,
12 Shanghai Key Lab for Urban Ecological Processes and Eco-Restoration, School of
13 Ecological and Environmental Sciences, East China Normal University, Shanghai
14 200241, China

15 ²BGI Genomics, BGI-Shenzhen, Shenzhen 518083, China

16 ³Agriculture & Environment Department, Harper Adams University, Newport, TF10
17 8NB, United Kingdom

18 ⁴CAS Key Laboratory of Tropical Forest Ecology, Xishuangbanna Tropical Botanical
19 Garden, Chinese Academy of Sciences, Mengla, Yunnan Province 666303, China

20 ⁵Ecological Security and Protection Key Laboratory of Sichuan Province, Mianyang
21 Normal University, Mianyang 621000, China

22 ⁶INRAE, UMR1062 CBGP, F-34988 Montferrier-sur-Lez, France

23 ⁷College of Life Sciences, Northwest University, Xi'an, Shaanxi 710069, China

24 ⁸Department of Biological and Marine Science, University of Hull, Hull HU6 7RX,
25 UK

26 ⁹CEFE, CNRS, Univ Montpellier, Univ Paul Valéry Montpellier, EPHE, IRD, France

27 ¹⁰School of Life Sciences, East China Normal University, Shanghai 200241, China

28 ¹¹Key Laboratory of Bio-resource and Eco-environment of Ministry of Education,
29 College of Life Sciences, Sichuan University, Chengdu 610065, China.

30 ¹²School of Life Sciences, Guangzhou University, Guangzhou 510006, China

31 ¹³Department of Biology, University of Maryland, College Park, MD 20742, The
32 United States of America

33 ¹⁴Department of Plant Biology, University of Illinois at Urbana-Champaign, Urbana,
34 IL 61801, USA

35 ¹⁵Center for Genomics and Biotechnology, Fujian Provincial Key Laboratory of
36 Haixia Applied Plant Systems Biology, Key Laboratory of Genetics, Breeding and
37 Multiple Utilization of Corps, Ministry of Education, Fujian Agriculture and
38 Forestry University, Fuzhou 350002, China.

39 ¹⁶Key Laboratory of the Ministry of Education for Coastal and Wetland Ecosystems,
40 College of the Environment and Ecology, Xiamen University, Xiamen, Fujian
41 361102, China

42 ¹⁷Key Laboratory of Plant Resource Conservation and Sustainable Utilization, South
43 China Botanical Garden, Chinese Academy of Sciences, Guangzhou 510650,
44 China

45 ¹⁸School of Life Sciences, Qufu Normal University, Qufu Shandong, 273165, China

46 ¹⁹School of Biology, University of Leeds, Leeds LS2 9JT, UK

47 ²⁰Shanghai Institute of Pollution Control and Ecological Security, Shanghai 200092,

48 China

49

50 † These authors contributed equally to this work.

51 * Co-corresponding authors.

52 E-mail: xychen@des.ecnu.edu.cn (X.-Y.C.); yuhui@scib.ac.cn (H.Y.);

53 S.G.A.Compton@leeds.ac.uk (S.G.C.); yuezhen@bgi.com (Z.Y.)

54

55 **Abstract**

56 Many insects metamorphose from antagonistic larvae into mutualistic adult
57 pollinators, with reciprocal adaptation leading to specialized insect-plant associations.
58 It remains unknown how such interactions are established at molecular level. Here we
59 assemble high-quality genomes of a fig species, *Ficus pumila* var. *pumila*, and its
60 specific pollinating wasp, *Wiebesia pumilae*. We combine multi-omics with validation
61 experiments to reveal molecular mechanisms underlying this specialized interaction.
62 In the plant, we identify the specific compound attracting pollinators and validate the
63 function of several key genes regulating its biosynthesis. In the pollinator, we find a
64 highly reduced number of odorant-binding protein (OBP) genes and an OBP mainly
65 binding the attractant. During antagonistic interaction, we find similar chemical
66 profiles and turnovers throughout the development of galled ovules and seeds, and a
67 significant contraction of detoxification-related gene families in the pollinator. Our
68 study identifies some key genes bridging coevolved mutualists, establishing
69 expectations for more diffuse insect-pollinator systems.

70

71 **Keywords**

72 Multi-omics, plant-pollinator mutualism, insect-host identification, pollinator
73 adaptation to host plant, gene for gene coadaptation

74

75 **Introduction**

76 Evolutionary adaptation fuels the genetic diversification of living organisms,
77 driving speciation and emergent biodiversity^{1,2}. However, in contrast to adaptation to
78 abiotic conditions³⁻⁵, it remains unclear how species adapt to reciprocally evolving
79 biotic factors at the molecular level. This reflects the difficulty of identifying the traits
80 linking interspecific interactions in a dynamic selective landscape. The high diversity
81 of phytophagous insects and angiosperms is believed to be the result of coevolution,
82 in part driven by ongoing insect-plant arms races^{6,7}. Many herbivorous insects are also
83 responsible for mediating gene flow between plant populations, often occurring as
84 both antagonistic (i.e., herbivorous) larvae and mutualistic pollinating adults⁸.
85 Selection by multiple agents associated with herbivorous/pollinating insects acts on
86 floral traits to both deter herbivores and attract pollinators⁹, making it difficult to
87 separate mechanistic processes in many plant-pollinator systems. Tightly co-evolved
88 species often have more apparent interacting traits, which provide an excellent testing
89 ground for exploring coadaptation.

90 The obligate mutualisms comprising ~800 species from the genus *Ficus*
91 (Moraceae) and their host specific pollinating wasps (fig wasps; Hymenoptera,
92 Agaonidae) form a classical example of coevolution and contribute greatly to
93 ecosystem functioning, biodiversity and agriculture^{10,11}. Both mutualists have evolved
94 strict correspondence in morphological, metabolic and life history traits^{10,12}. The
95 plants reward the larvae of pollinating wasps with nutrition and protection, and each
96 mutualist wasp species is both pollinator and herbivore¹². Each individual wasp

97 spends the majority of its lifespan at the larval stage (from three weeks up to nine
98 months) and develops inside a single galled ovule of a female floret located inside the
99 enclosed inflorescences characteristic of the genus (figs or ‘syconia’)¹³⁻¹⁵ (Fig. 1a).
100 There are two predominant types of breeding systems in *Ficus* species, monoecy and
101 dioecy¹⁶. In monoecious figs, each fig produces female florets that can be either
102 pollinated or galled by pollinator larvae. In dioecious species, only the female florets
103 (feeder florets) in figs of functional male trees support the development of pollinator
104 offspring; figs growing on female trees attract pollinators to fertilize the female florets
105 (seed florets) that do not support wasp development (Fig. 1a). Upon locating host figs,
106 adult female wasps must crawl through a narrow passage usually lined by bracts (the
107 ostiole), into a dark central lumen where they typically remain trapped following
108 oviposition and/or pollination. Short lived (usually shorter than three days) adult
109 wasps do not feed¹⁰.

110 Central to mediating these species-specific interactions are plant-emitted volatile
111 organic compounds (VOCs), which guide adult female wasps to precisely identify and
112 locate host figs^{13,14,17-21}. Moreover, the high-quality genomes of a *Ficus* species and its
113 pollinating wasp (*Ficus microcarpa* and *Eupristina verticillata*) have been recently
114 reported¹¹, which create a basis for exploring how these pollinators identify host figs
115 at the molecular level. However, to date the key attractive VOCs have only been
116 explicitly identified in a small number of fig-pollinator mutualisms^{17,18}, and the
117 underlying molecular mechanisms determining host-specific signaling and insect
118 attraction remain unknown.

119 Once the problem of host identification has been overcome, pollinator larvae
120 must also survive and develop under a set of unique conditions inside galled ovules
121 that support their development (Fig. 1a). While figs can defend against herbivores
122 from a wide range of taxa²², it is unclear how pollinator larvae cope with plant
123 defensive chemicals inside the galled ovules during this antagonistic phase of
124 mutualism. One possible explanation is that galling behavior may activate the plant
125 reproductive program in galled tissues, so that galling insects can avoid the strong
126 chemical defenses induced by stress reaction when they utilize plant nutrients²³⁻²⁵. To
127 test whether the reproductive program is activated in galled ovules, it is necessary to
128 compare between the chemical profiles of galled ovules and seeds. We also expect
129 that such adaptation to a specialized environment must leave molecular footprints in
130 pollinator genome, for example contracted detoxification-related gene families^{26,27}.

131 Here we focused on a fig-pollinator mutualism comprising a dioecious *Ficus*
132 species *Ficus pumila* var. *pumila*²⁸ and its specific pollinator *Wiebesia pumilae*²⁹ (Fig.
133 1a). We used multi-omics in combination with validation experiments to unravel the
134 key molecular mechanisms contributing to the antagonistic and the mutualistic
135 interactions in this system. We determined the specific attractive VOC and several key
136 genes relevant to its biosynthesis. We identified the corresponding responses in the
137 odorant-binding protein (OBP) genes in the pollinator genome and an OBP mainly
138 binding the attractant. During the antagonistic phase, we found a similar turnover of
139 secondary metabolites when female florets developed into either galled ovules or
140 seeds, and almost identical chemical profiles between these two tissues. It implies that

141 the galled ovules may develop like seeds. A contraction of detoxification-related gene
142 families was found in the pollinator genome, providing insights into the fig-pollinator
143 coadaptation during antagonistic interaction.

144 **Results**

145 **Assembly of genomes and evolution**

146 To provide high-quality reference genomes for transcriptomic and proteomic
147 analyses, we assembled genomes of *F. pumila* var. *pumila* and *W. pumilae* using a
148 combination of Illumina and PacBio sequencing technologies (Supplementary Table
149 1; see Methods). The assembled genomes were 315.7 Mb (contig N50 of 2.3 Mb) for
150 the plant and 318.2 Mb (contig N50 of 10.9 Mb) for the pollinator (Table 1 and
151 Supplementary Table 2). Using the uniquely mapped reads produced by the high-
152 throughput chromatin conformation capture (Hi-C) technique (Supplementary Tables
153 1, 2), we generated Hi-C-based physical maps composed of 13 and 6 pseudo-
154 chromosomes, with 96.6% (305 Mb) and 99.8% (318 Mb) of the assembled genomes
155 anchored to the pseudo-chromosomes (Table 1 and Supplementary Fig. 1). The
156 scaffold N50 of the assembled genomes were 22.4 Mb and 59.4 Mb, and the pseudo-
157 chromosomes included 97.1% (27,378) and 99.8% (12,292) of protein-coding genes
158 (Table 1). Genome annotation results showed that the structures and functions of
159 25,905 and 12,305 protein-coding genes were annotated in the two genomes
160 (Supplementary Figs. 2 and Supplementary Tables 3-5). BUSCO quality analysis of
161 annotation showed that 92.4% of 1375 conserved plant genes and 91.3% of 4,415
162 Hymenoptera genes have complete coverage (Supplementary Table 3).

163 The protein-coding genes of *F. pumila* var. *pumila* and *W. pumilae* were clustered
164 into 15,631 and 7,969 gene families (Supplementary Fig. 3 and Supplementary Table
165 6). Analysis of comparative genomics using the genomes of 13 Angiosperm species
166 including *F. pumila* var. *pumila* and three congeneric species (*Ficus hispida*¹¹, *Ficus*
167 *microcarpa*¹¹ and *Ficus carica*¹⁶) showed that in the common ancestors of the four
168 *Ficus* species, 1,473 gene families had contracted and 888 gene families had
169 expanded. Phylogenetic reconstruction revealed that *F. hispida* is more closely related
170 to *F. pumila* var. *pumila* than the other two *Ficus* species (Supplementary Fig. 4a). In
171 the analysis of comparative genomics using the genomes of 11 arthropod species
172 containing *W. pumilae* and two other pollinator wasp species (*Ceratosolen solmsi*¹¹
173 and *Eupristina verticillata*²⁷), we found 48 expanded and 1261 contracted gene
174 families in the common ancestors of three pollinating wasp species. We recovered a
175 group containing *E. verticillata* and *W. pumilae* with *C. solmsi* as its sibling
176 (Supplementary Fig. 4b). There was no evidence for recent whole-genome duplication
177 in the plant, and only a few small segments (total length of 1.3 Mb) were found to be
178 duplicated in the pollinator genome (Supplementary Fig. 5).

179 **Attractive compound forming fig-pollinator identification**

180 At the receptive stage, figs release VOCs containing critical compound(s)
181 attracting their pollinating wasps (Fig. 1a). To determine the attractive compound(s),
182 we collected VOCs from functional male and female figs of *F. pumila* var. *pumila* at
183 the pre-repetitive and the receptive stages using the dynamic headspace sampling
184 (DHS) approach, and identified a total of 70 compounds (Fig. 1a and Supplementary

185 Tables 7, 8). Only three (linalool, nonanal and decanal) of these compounds were
186 found to elicit physiological responses of adult females of *W. pumilae* (Fig. 1b, c), of
187 which only decanal was emitted exclusively at the receptive stage (Supplementary
188 Table 8). We then conducted behavioral preference tests among the three compounds
189 using 50 female pollinating wasps in each testing group. The wasps showed a
190 significantly greater preference for decanal than the control and a significantly
191 reduced preference for nonanal than the control, with a similar preference between
192 decanal and a nonanal-decanal blend (Fig. 1d and Supplementary Table 9). These
193 results demonstrate that the VOC compound decanal, emitted by *F. pumila* var. *pumila*
194 figs at the receptive stage, functions to attract the pollinating wasp *W. pumilae*.

195

196 **Molecular mechanisms of specific host identification**

197 To identify the molecular mechanisms underlying the behavioral responses of *W.*
198 *pumilae* to the VOCs emitted by its host figs, we annotated the four gene families
199 involved in insect olfaction³⁰. Across these gene families, *W. pumilae*, *E. verticillata*
200 and *C. solmsi* consistently have lower numbers of genes, and, in particular, the
201 number of odorant-binding protein (OBP) genes is significantly lower than less host-
202 specific insects (Fig. 2a). Phylogenetic and synteny analysis including genomes of the
203 three pollinating wasp species and the distantly related *Nasonia vitripennis* showed
204 that most OBP genes in the pollinating wasp species displayed strong homology and
205 that the small number of OBP genes resulted from gene loss and infrequent tandem
206 duplication (Supplementary Figs. 6a, 7a). There were apparent differences in motif

207 structure among OBPs in six of the ten syntenic blocks (Supplementary Fig. 6b). The
208 general contraction in OBP genes and frequent changes in motif structure of
209 homologous OBPs among pollinating wasp species may be expected given their high
210 host specificity and different VOC cues used for detecting host figs.

211 Among the 12 OBP genes of *W. pumilae*, transcriptome and proteome evidence
212 showed that all genes were transcribed but only seven are translated into detectable
213 proteins in adult females (Fig. 2b, Supplementary Fig. 8 and Supplementary Table 7).
214 There were no proteins with significant differences in quantity (PSDs) and
215 differentially expressed genes (DEGs) between the control and the VOCs-contacting
216 treatment (Supplementary Table 10).

217 To explore functions of *W. pumilae* OBPs, we predicted motif structures of OBPs
218 and compared them with the OBPs in *Adelphocoris lineolatus*³¹ and *Culex*
219 *quinquefasciatus*³², known to have decanal or nonanal binding activity. Among the
220 seven OBPs with detectable protein products, WpumOBP2 shows similar structure to
221 the known decanal-binding protein and WpumOBP11 is similar to the known
222 nonanal-binding protein (Fig. 2c and Supplementary Fig. 9). To validate the functions
223 of WpumOBP2 and WpumOBP11, we produced the recombinant proteins for these
224 two OBPs and measured their binding affinity to decanal and nonanal using surface
225 plasmon resonance (SPR) experiments. Consistent with the prediction, the
226 experiments revealed considerably lower K_D (representing much higher binding
227 affinity) of WpumOPB2 to decanal than to nonanal and far lower K_D of WpumOBP11
228 to nonanal than to decanal, and thus demonstrate the high binding affinity of these two

229 OBPs to the corresponding compounds (Fig 2d, Supplementary Fig. 10 and
230 Supplementary Table 11). Therefore, these results provide solid evidence that
231 WpumOBP2 is the main binding protein to the attractant, and pollination of *F. pumila*
232 *var. pumila* by *W. pumilae* is initiated by the binding of decanal with WpumOPB2.

233

234 **Regulation of gene expression in attractant biosynthesis**

235 To identify the tissue for attractant emission within figs, we measured the
236 concentration of decanal emitted by ostiolar tissues and female florets at the receptive
237 stage from both sexes of *F. pumila var. pumila* (Fig. 1a) using DHS, as previous
238 studies from other species suggested VOCs are mainly released from these tissues^{13,20}.
239 The concentration of collected decanal in ostiolar tissues was 3.13 ± 1.11 pg/g, which
240 was 9.1 times as that in female florets (0.34 ± 0.05 pg/g) (Pairwise T Test: df=9,
241 $t=6.02$, $p=0.002$). Thus, the results revealed that decanal was predominantly emitted
242 by ostiolar tissues at a similar concentration between sexes (T Test: df=4, $t=0.20$,
243 $p=0.858$ in ostiolar tissues; df=4, $t=0.24$, $p=0.826$ in female florets).

244 To identify key genes involved in the biosynthesis of decanal, we conducted
245 transcriptome and proteome analyses on ostiolar tissues collected at the pre-receptive
246 and the receptive stages (Supplementary Table 7). The biosynthesis of decanal and
247 nonanal is involved in the pathways of fatty acid biosynthesis (ko00061), elongation
248 (ko00062) and metabolism (ko00071 and ko00592) (Fig. 3a)^{33,34}. Genes in these
249 pathways showed similar patterns of expression between transcriptome and proteome
250 data (Supplementary Fig. 11 and Supplementary Table 12). Comparing the receptive

251 with the pre-receptive stage, we detected a total of eight PSDs (Fig. 3b), likely
252 facilitating the biosynthesis of decanal and suppressing the biosynthesis of nonanal at
253 the receptive stage (Fig. 3a). Down-regulated PSDs included two ACSLs (long-chain
254 acyl-CoA synthetase) and one HACD (very-long-chain (3R)-3-hydroxyacyl-CoA
255 dehydratase), while up-regulated PSDs comprised an ALDH (acetaldehyde
256 dehydrogenase), an ADH (alcohol dehydrogenase), two LOX2Ss (lipoxygenase) and
257 one HPL (hydroperoxide lyase) (Fig. 3b). To validate the function of key genes (the
258 two ACSLs, the ALDH and the ADH) in decanal biosynthesis, we produced the
259 recombinant proteins of these genes and conducted *in vitro* enzyme activity assay (see
260 Methods). The final products of the *in vitro* reactions identified by LC-MS or GC-
261 MS are consistent with the standards (Fig. 3 c-e). These results validate the enzyme
262 activity of the two ACSLs in synthesizing hexadecanoyl-CoA as well as the ALDH
263 and the ADH in synthesizing decanal and decanol.

264 To understand the transcriptional regulation of decanal biosynthesis, we
265 conducted co-expression network analysis and found one module containing two key
266 genes (*FpumACSL10* and *FpumALDH1*) and four potential regulating transcription
267 factors (two *HD-ZIPs*, one *bHLH* and one *bZIP*) (Fig. 3f and Supplementary Table
268 13). Cis-element detection analysis revealed one G-box motif upstream of
269 *FpumACSL10* and six G-box and one HD-Zip motifs upstream of *FpumALDH1*
270 (Supplementary Table 14). As G-box binds to transcription factor families of bZIPs
271 and bHLHs and HD-Zip binds to HD-ZIPs^{35,36}, we hypothesized that expression of
272 *FpumACSL10* is regulated by the bHLH and the bZIP and all above four transcription

273 factors regulate the expression of *FpumALDH1*. To test this hypothesis, we obtained
274 qualified polyclonal antibodies for the four transcription factors and performed ChIP-
275 qPCR experiments. High % input and fold enrichment values showed that the bHLH
276 and the bZIP could bind to the promoter region of *FpumACSL10* and all the four
277 transcription factors could bind to the promoter region of *FpumALDH1* (Fig. 3g, h),
278 providing evidence for our hypothesis.

279

280 **Metabolic and genomic signature of antagonistic interaction**

281 To understand the mechanisms of antagonistic interaction between figs of *F.*
282 *pumila* var. *pumila* and larvae of *W. pumilae*, we analyzed chemical profiles of
283 different tissue types of female and functional male figs at the receptive and the post-
284 receptive stage using metabolomic data (Supplementary Table 7; see Methods). We
285 focused on the secondary metabolites associated with plant chemical defenses
286 (SMCDs)^{22,37-39}, comprising some terpenoids (triterpenes and sesquiterpenes) and
287 phenylpropanoids (including their precursors and their derivatives) (Supplementary
288 Fig. 12). Metabolomic analysis revealed 736 SMCDs (108 terpenoids and 628
289 phenylpropanoids) (Supplementary Table 15). While we found significant differences
290 in chemical profiles between two types of tissues and between different fig
291 development stages, there were few differences between female and functional male
292 figs (Fig. 4a). No secondary metabolites with significant difference in quantity
293 (SMSDs) were found between feeder and seed florets at the receptive stage, and there
294 were only three SMSDs between galled ovules and seeds at the post-receptive stage

295 (Fig. 4b). Remarkably, we found similar changes of SMSDs in both the feeder floret-
296 galled ovule and the seed floret-seed transitions (Fig. 4c and Supplementary Fig. 13a).
297 Besides SMCDs, galled ovules and seeds shared similar overall chemical profiles
298 (Supplementary Fig. 14). These results showed similar chemical changes and profiles
299 in the development of female florets no matter they were parasitized by pollinator
300 larvae (becoming galled ovules) or not (developing into seeds).

301 As might be expected from organisms that spend most their lives in a specific
302 environment, contraction of three gene families crucial to the detoxification of plant
303 defensive chemicals⁴⁰ (CYP450s, glutathione s-transferases (GSTs) and
304 carboxylesterases (CCEs) gene families) was found in the genomes of *W. pumilae*, *E.*
305 *verticillata* and *C. solmsi* (Fig. 4d and Supplementary Fig. 15). Such contraction was
306 mainly caused by gene loss and infrequent tandem duplication (Supplementary Fig.
307 7b-d), and most of the detoxification-related genes in the three pollinating wasp
308 species were in the same monophyletic groups (Supplementary Fig. 16). Ten out of
309 the 56 detoxification-related genes in *W. pumilae* was at a high level (read counts >
310 200) and was significantly upregulated at the larval stage compared to the adult stage
311 (Supplementary Fig. 17 and Supplementary Table 16). These metabolic and genomic
312 signatures provide a molecular basis for further exploring the mechanisms of fig-
313 pollinator coadaptation during their antagonistic interaction.

314 **Discussion**

315 Reciprocal selection on signaling and defense traits has shaped the molecular
316 constraints governing how antagonistic larvae develop into mutualistic adult

317 pollinators^{8,41}. In this study, our combination of classic electrophysiological
318 experiments and multi-omics approaches has illuminated some key mechanisms
319 forming the coadaptation in a pair of fig-pollinator mutualists. We identified the
320 attractive VOC, detected that host identification by the specific pollinators may be
321 linked to their reduced number of OBP genes, and validated an OBP mainly binding
322 the attractant. We identified the key genes involved in the regulation of both attractant
323 and repellent biosynthesis in the plant: from facilitating the synthesis of the repellent
324 to favoring the production of the attractant. Surprisingly, matched changes in SMCDs
325 occurred across the transitions from i) floret to galled ovule and ii) floret to seed, and
326 almost identical profiles of SMCDs were found in galled ovules and seeds. As for the
327 pollinator, we detected a contraction of detoxification-related gene families.

328 Previous studies have mainly focused on the dominant components or the
329 bouquet of components in the VOCs emitted by figs^{14,17}. In contrast our results
330 showed that only one VOC of relative low concentration attracts the focal pollinating
331 wasp species, addressing the importance of detailing the complete spectrum of VOCs.
332 Moreover, the attractive VOC (an aldehyde) in our focal species is distinct from the
333 attractants found in other *Ficus* species (usually terpenes)^{11,13,14,17,18}. Such a dramatic
334 difference indicates deep divergence among congeners in the recognition of VOC
335 attractants^{42,43}, providing the basis for adaptive radiations in both *Ficus* and their
336 pollinating wasps⁴⁴. In addition, similar concentration of the attractant emitted by
337 different sexes of figs supports the intersexual mimicry hypothesis in *Ficus* species²¹,
338 which argues that any changes in biosynthesis of attractant VOCs in female figs may

339 cause loss of sexual reproduction²¹.

340 Similar chemical changes in the development of galled ovules and seeds and
341 almost identical SMCD profiles in these tissues showed that the occupancy of
342 pollinator larvae activates the reproductive program of galled ovules. This suggests
343 that galling strategy may help pollinator larvae avoid the potential chemical sanctions
344 when they exploit nutrients of host plants. This is likely to result from either pollinator
345 larvae manipulating plant physiology or changes triggered by host figs once the feeder
346 florets are galled. Chemical mimicry of fruits and seeds has been reported in other
347 galling insects^{24,25}, while many studies also suggest that figs have evolved to
348 accommodate pollinator larvae^{10,15}. Other possibilities, such as pollination before
349 oviposition combined with minimal initial interference of pollinator larvae can be
350 largely excluded, because most galled ovules were not pollinated. Furthermore, we
351 collected figs at the middle (four weeks after the entrance of pollinator foundresses) of
352 the post-receptive stage (generally lasting 8-10 weeks). Future research should
353 perform bioassays to determine the chemicals inducing the development of galled
354 ovules and the specific secondary metabolites defending against pollinator larvae.
355 This will reveal how pollinator larvae activate the reproductive programs of host
356 plants and why they can only utilize feeder florets.

357 The pollinating wasp species have evolved specializations in OBP and
358 detoxification-related genes, probably because they are host specific and spend most
359 of their lives inside galled ovules (though some detoxification-related genes are not
360 only involved in detoxification but also important for the general life cycle of insects).

361 Such specializations facilitate the maintenance of host-specificity, but conservation of
362 some OBP genes among pollinating wasps (Supplementary Figs. 6, 7) may also offer
363 opportunities for host shift^{19,45,46}. Moreover, selection to maximize pollinator fitness
364 may drive rapid adaptive changes in fig traits like floral scents, and such reciprocal
365 selection has occurred in some generalized plant-pollinator systems⁴⁷.

366 Ongoing global changes are causing rapid evolution and phenotypic changes in
367 many plants, leading to mismatches between key traits bridging plants and their
368 pollinators^{4,48}. Erosion of these links can result in the collapse of long-evolved
369 mutualisms and a loss of biodiversity, but may also lead to the rewiring of host
370 association networks^{4,49,50}. Limitations to our knowledge of molecular determination
371 in plant-pollinator interactions have made predictions about future changes in
372 biodiversity and ecosystem functioning largely speculative. Our findings offer an
373 example of gene for gene coadaptation that extends beyond the existing phenotype-
374 based models of mutualism persistence⁵¹ and place trait-based multi-omics at the
375 center of the ecological and evolutionary research concerning interacting species in
376 more diffuse systems.

377 **References**

- 378 1. Lamichhaney, S. et al. Evolution of Darwin's finches and their beaks revealed by
379 genome sequencing. *Nature* **518**, 371–375 (2015).
- 380 2. Simões, M. et al. The evolving theory of evolutionary radiations. *Trends Ecol.*
381 *Evol.* **31**, 27–34 (2016).
- 382 3. Arnegard, M. E. et al. Genetics of ecological divergence during speciation.

- 383 *Nature* **511**, 307–311 (2014).
- 384 4. Hoffmann, A. A. & Sgrò, C. M. Climate change and evolutionary adaptation.
385 *Nature* **470**, 479–485 (2011).
- 386 5. Olsen, J. L. et al. The genome of the seagrass *Zostera marina* reveals angiosperm
387 adaptation to the sea. *Nature* **530**, 331–335 (2016).
- 388 6. Becerra, J. X., Nogueb, K. & Venable, D. L. Macroevolutionary chemical
389 escalation in an ancient plant–herbivore arms race. *Proc. Natl. Acad. Sci. USA*
390 **106**, 18062–18066 (2009).
- 391 7. Edger, P. P. et al. The butterfly plant arms-race escalated by gene and genome
392 duplications. *Proc. Natl. Acad. Sci. USA* **112**, 8362–8366 (2015).
- 393 8. Adler, L. S. & Bronstein, J. L. Attracting antagonists: does floral nectar increase
394 leaf herbivory? *Ecology* **85**, 1519–1526 (2004).
- 395 9. McCall, A. C. & Irwin, R. E. Florivory: the intersection of pollination and
396 herbivory. *Ecol. Lett.* **9**, 1351–1365 (2006).
- 397 10. Cook, J. M. & Rasplus, J.-Y. Mutualists with attitude: coevolving fig wasps and
398 figs. *Trends Ecol. Evol.* **18**, 241–248 (2003).
- 399 11. Zhang, X. et al. Genomes of the banyan tree and pollinator wasp provide insights
400 into fig-wasp coevolution. *Cell* **183**, 1–15 (2020).
- 401 12. Herre, E. A., Jandér, K. C. & Machado, C. A. Evolutionary ecology of figs and
402 their associates: recent progress and outstanding puzzles. *Annu. Rev. Ecol. Evol.*
403 *Syst.* **39**, 439–458 (2008).
- 404 13. Souza, C. D. et al. Diversity of fig glands is associated with nursery mutualism in

- 405 fig trees. *Am. J. Bot.* **102**, 1564–1577 (2015).
- 406 14. Souto-Vilarós, D. et al. Pollination along an elevational gradient mediated both by
407 floral scent and pollinator compatibility in the fig and fig-wasp mutualism. *J.*
408 *Ecol. Evol.* **106**, 2256–2273 (2018).
- 409 15. Wang, R. et al. Loss of top-down biotic interactions changes the relative benefits
410 for obligate mutualists. *Proc. R. Soc. B.* **286**, 20182501 (2019).
- 411 16. Mori K. et al. Identification of RAN1 orthologue associated with sex
412 determination through whole genome sequencing analysis in fig (*Ficus carica L.*).
413 *Sci. Rep.* **7**, 41124 (2017).
- 414 17. Proffit M. et al. Chemical signal is in the blend: bases of plant-pollinator
415 encounter in a highly specialized interaction. *Sci. Rep.* **10**, 10071 (2020).
- 416 18. Chen, C. et al. Private channel: a single unusual compound assures specific
417 pollinator attraction in *Ficus semicordata*. *Funct. Ecol.* **23**, 941–950 (2009).
- 418 19. Wang, G., Cannon, C. H. & Chen, J. Pollinator sharing and gene flow among
419 closely related sympatric dioecious fig taxa. *Proc. R. Soc. B.* **283**, 20152963
420 (2016).
- 421 20. Yu, H. et al. De novo transcriptome sequencing in *Ficus hirta* Vahl. (Moraceae) to
422 investigate gene regulation involved in the biosynthesis of pollinator attracting
423 volatiles. *Tree Genet. Genomes* **11**, 91 (2015).
- 424 21. Soler, C. C. L., Proffit, M., Bessière, J.-M., Hossaert -McKey, M. & Schatz, B.
425 Evidence for intersexual chemical mimicry in a dioicous plant. *Ecol. Lett.* **15**,
426 978–985 (2012).

- 427 22. Volf, M. et al. Community structure of insect herbivores is driven by
428 conservatism, escalation and divergence of defensive traits in *Ficus*. *Ecol. Lett.*
429 **21**, 83–92 (2018).
- 430 23. Martinson, E.O., Hackett, J.D., Machado, C.A. & Arnold A.E. Metatranscriptome
431 analysis of fig flowers provides insights into potential mechanisms for mutualism
432 stability and gall induction. *PLoS ONE* **10**, e0130745 (2015).
- 433 24. Zhang, H. et al. Leaf-mining by *Phyllonorycter blancardella* reprograms the host-
434 leaf transcriptome to modulate phytohormones associated with nutrient
435 mobilization and plant defense. *J. Insect Physiol.* **84**, 114–127 (2016).
- 436 25. Schultz, J.C., Edger, P.P., Body, M. & Appel, H.M. A galling insect activates plant
437 reproductive programs during gall development. *Sci. Rep.* **9**, 1833 (2019).
- 438 26. The *Nasonia* Genome Working Group. Functional and evolutionary insights from
439 the genomes of three parasitoid *Nasonia* species. *Science* **327**, 343–348 (2010).
- 440 27. Xiao, J.-H. et al. Obligate mutualism within a host drives the extreme
441 specialization of a fig wasp genome. *Genome Biol.* **14**, R141 (2013).
- 442 28. Ohri, D. & Khoshoo, T. N. Nuclear DNA contents in the genus *Ficus* (Moraceae).
443 *Plant Syst. Evol.* **156**, 1–4 (1987).
- 444 29. Chen, Y., Compton, S. G., Liu, M. & Chen, X.-Y. Fig trees at the northern limit of
445 their range: the distributions of cryptic pollinators indicate multiple glacial
446 refugia. *Mol. Ecol.* **21**, 1687–1701 (2012).
- 447 30. Chen, L.-G. et al. Binding affinity characterization of an antennae-enriched
448 chemosensory protein from the white-backed planthopper, *Sogatella furcifera*

- 449 (Horváth), with host plant volatiles. *Pestic. Biochem. Phys.* **152**, 1–7 (2018).
- 450 31. Gu, S.-H. et al. Functional characterization and immunolocalization of odorant
451 binding protein 1 in the lucerne plant bug, *Adelphocoris lineolatus* (GOEZE).
452 *Arch. Insect Biochem.* **77**, 81–98 (2011).
- 453 32. Leal, W. S. et al. Reverse and conventional chemical ecology approaches for the
454 development of oviposition attractants for *Culex* mosquitoes. *PLoS ONE* **3**, e3045
455 (2008).
- 456 33. Rizzo, W. B. et al. Fatty aldehyde and fatty alcohol metabolism: review and
457 importance for epidermal structure and function. *BBA-Mol. Cell Biol. L.* **1841**,
458 377–389 (2014).
- 459 34. Schwab, W., Davidovich-Rikanati, R. & Lewinsohn, E. Biosynthesis of plant-
460 derived flavor compounds. *Plant J.* **54**, 712–732 (2008).
- 461 35. Capella, M., Ribone, P. A., Arce, A. L. & Chan, R. L. *Arabidopsis thaliana*
462 HomeoBox 1 (AtHB1), a Homeodomain-Leucine Zipper I (HD-Zip I) transcription
463 factor, is regulated by PHYTOCHROME-INTERACTING FACTOR 1 to
464 promote hypocotyl elongation. *New Phytol.* **207**, 669–682 (2015).
- 465 36. Jiang, W. et al. Two transcription factors TaPpm1 and TaPpb1 co-regulate
466 anthocyanin biosynthesis in purple pericarps of wheat. *J. Exp. Bot.* **69**, 2555–
467 2567 (2018).
- 468 37. Guan, R. et al. Draft genome of the living fossil *Ginkgo biloba*. *GigaScience* **5**,
469 49 (2016).
- 470 38. Mithöfer, A., & Boland, W. Plant defense against herbivores: chemical aspects.

- 471 *Annu. Rev. Plant Biol.* **63**, 431–450 (2012).
- 472 39. Salazar, D. et al. Origin and maintenance of chemical diversity in a species-rich
473 tropical tree lineage. *Nat. Ecol. Evol.* **2**, 983–990 (2018).
- 474 40. Després, L., David, J. P. & Gallet, C. The evolutionary ecology of insect
475 resistance to plant chemicals. *Trends Ecol. Evol.* **22**, 298–307 (2007).
- 476 41. Segar, S. T., Volf, M., Sisol, M., Pardikes, N. & Souto-Vilarós, A. D. Chemical
477 cues and genetic divergence in insects on plants: conceptual cross pollination
478 between mutualistic and antagonistic systems. *Curr. Opin. Insect Sci.* **32**, 83–90
479 (2019).
- 480 42. Cook, J. M. & Segar, S. T. Speciation in fig wasps. *Ecol. Entomol.* **35**, 54–66
481 (2010).
- 482 43. Cruaud, A. et al. An extreme case of plant-insect codiversification: figs and fig-
483 pollinating wasps. *Syst. Biol.* **61**, 1029–1047 (2012).
- 484 44. Yu, H. et al. Multiple parapatric pollinators have radiated across a continental fig
485 tree displaying clinal genetic variation. *Mol. Ecol.* **28**, 2391–2405 (2019).
- 486 45. Satler, J. D. et al. Inferring processes of coevolutionary diversification in a
487 community of Panamanian strangler figs and associated pollinating wasps.
488 *Evolution* **73**, 2295–2311 (2019).
- 489 46. Wang, G. et al. Genomic evidence of prevalent hybridization throughout the
490 evolutionary history of the fig-wasp pollination mutualism. *Nat. Commun.* **12**,
491 718 (2021).
- 492 47. Hoballah, M. E. et al. Single gene-mediated shift in pollinator attraction in

- 493 Petunia. *Plant Cell* **19**, 779–790 (2007).
- 494 48. Potts, S. G. et al. Global pollinator declines: trends, impacts and drivers. *Trends*
495 *Ecol. Evol.* **25**, 345–353 (2010).
- 496 49. Kiers, E. T., Palmer, T. M., Ives, A. R., Bruno, J. F. & Bronstein, J. L. Mutualisms
497 in a changing world: an evolutionary perspective. *Ecol. Lett.* **13**, 1459–1474
498 (2010).
- 499 50. Segar, S. T., Fayle, T. M., Srivastava, D. S., Lewinsohn, T. M., Lewis, O. T.,
500 Novotny, V., Kitching, R. L. & Maunsell, S. C. The role of evolution in shaping
501 ecological networks. *Trends Ecol. Evol.* **35**, 454–466 (2020).
- 502 51. Stoy, K. S., Gibson, A. K., Gerardo, N. M. & Morran, L. T. A need to consider the
503 evolutionary genetics of host-symbiont mutualisms. *J Evol. Biol.* **33**, 1656–1668
504 (2020).
- 505 52. Marçais, G. & Kingsford, C. A fast, lock-free approach for efficient parallel
506 counting of occurrences of k-mers. *Bioinformatics* **27**, 764–770 (2011).
- 507 53. Xiao, C.-L. et al. MECAT: fast mapping, error correction, and de novo assembly
508 for single-molecule sequencing reads. *Nat. Methods* **14**, 1072–1074 (2017).
- 509 54. Walker, B. J. et al. Pilon: an integrated tool for comprehensive microbial variant
510 detection and genome assembly improvement. *PLoS One* **9**, e112963 (2014).
- 511 55. Prysycz, L. P., & Gabaldón, T. Redundans: an assembly pipeline for highly
512 heterozygous genomes. *Nucleic Acids Res.* **44**, e113 (2016).
- 513 56. Zhang, Z., Schwartz, S., Wagner, L. & Miller, W. A greedy algorithm for aligning
514 DNA sequences. *J. Comput. Biol.* **7**, 203–214 (2000).

- 515 57. English, A. C. et al. Mind the gap: upgrading genomes with Pacific Biosciences
516 RS long-read sequencing technology. *PLoS ONE* **7**, e47768 (2012).
- 517 58. Sahlin, K., Chikhi, & Arvestad, R. L. Assembly scaffolding with PE-
518 contaminated mate-pair libraries. *Bioinformatics* **32**, 1925–1932 (2016).
- 519 59. Belton, J. M. et al. Hi-C: a comprehensive technique to capture the conformation
520 of genomes. *Methods* **58**, 268–276 (2012).
- 521 60. Servant, N. et al. (2015) HiC-Pro: an optimized and flexible pipeline for Hi-C
522 data processing. *Genome Biol.* **16**, 259.
- 523 61. Durand, N.C. et al. Juicer provides a one-click system for analyzing loop-
524 resolution Hi-C experiments. *Cell Syst.* **3**, 95–98 (2016).
- 525 62. Dudchenko, O. et al. De novo assembly of the *Aedes aegypti* genome using Hi-C
526 yields chromosome-length scaffolds. *Science* **356**, 92–95 (2017).
- 527 63. Simão, F. A., Waterhouse, R. M., Ioannidis, P., Kriventseva, E. V. & Zdobnov, E.
528 M. BUSCO: assessing genome assembly and annotation completeness with
529 single-copy orthologs. *Bioinformatics* **31**, 3210–3212 (2015).
- 530 64. Wu, T. D. & Watanabe, C. K. GMAP: a genomic mapping and alignment program
531 for mRNA and EST sequences. *Bioinformatics* **21**, 1859–1875 (2005).
- 532 65. Benson, G. Tandem repeats finder: a program to analyze DNA sequences. *Nucleic
533 Acids Res.* **27**, 573–580 (1999).
- 534 66. Bao, W., Kojima, K. K. & Kohany, O. Repbase Update, a database of repetitive
535 elements in eukaryotic genomes. *Mobile DNA* **6**, 11 (2015).
- 536 67. Xu, Z. & Wang, H. LTR_FINDER: an efficient tool for the prediction of full-

- 537 length LTR retrotransposons. *Nucleic Acids Res.* **35**, W265–W268 (2007).
- 538 68. Edgar, R. C. & Myers, E. W. PILER: identification and classification of genomic
539 repeats. *Bioinformatics* **21**, i152–i158 (2005).
- 540 69. Price, A. L., Jones, N. C. & Pevzner, P. A. De novo identification of repeat
541 families in large genomes. *Bioinformatics* **21**, i351–i358 (2005).
- 542 70. Lowe, T. M. & Eddy, S. R. tRNAscan-SE: a program for improved detection of
543 transfer RNA genes in genomic sequence. *Nucleic Acids Res.* **25**, 955–964
544 (1997).
- 545 71. Nawrocki, E. P. & Eddy, S. R. Infernal 1.1: 100-fold faster RNA homology
546 searches. *Bioinformatics* **29**, 2933–2935 (2013).
- 547 72. Nawrocki, E.P. et al. Rfam 12.0: updates to the RNA families database. *Nucleic
548 Acids Res.* **43**, D130–D137 (2015).
- 549 73. Holt, C. & Yandell, M. MAKER2: an annotation pipeline and genome-database
550 management tool for second-generation genome projects. *BMC Bioinformatics*
551 **12**, 491 (2011).
- 552 74. Kim, D., Langmead, B. & Salzberg, S.L. HISAT: a fast spliced aligner with low
553 memory requirements. *Nat. Methods* **12**, 357–360 (2015).
- 554 75. Pertea, M. et al. StringTie enables improved reconstruction of a transcriptome
555 from RNA-seq reads. *Nat. Biotechnol.* **33**, 290–295 (2015).
- 556 76. Johnson, A. D. et al. SNAP: a web-based tool for identification and annotation of
557 proxy SNPs using HapMap. *Bioinformatics* **24**, 2938–2939 (2008).
- 558 77. Stanke, M. & Morgenstern, B. AUGUSTUS: a web server for gene prediction in

- 559 eukaryotes that allows user-defined constraints. *Nucleic Acids Res.* **33**, W465–
560 W467 (2005).
- 561 78. Buels, R. et al. JBrowse: a dynamic web platform for genome visualization and
562 analysis. *Genome Biol.* **17**, 66 (2016).
- 563 79. Buchfink, B., Xie, C. & Huson, D.H. Fast and sensitive protein alignment using
564 DIAMOND. *Nat. Methods* **12**, 59–60 (2015).
- 565 80. Bairoch, A. & Apweiler, R. The SWISS-PROT protein sequence database and its
566 supplement TrEMBL in 2000. *Nucleic Acids Res.* **28**, 45–48 (2000).
- 567 81. Kanehisa, M., Sato, Y., Kawashima, M., Furumichi, M. & Tanabe, M. KEGG as a
568 reference resource for gene and protein annotation. *Nucleic Acids Res.* **44**, D457–
569 D462 (2016).
- 570 82. Jones, P. et al. InterProScan 5: genome-scale protein function classification.
571 *Bioinformatics* **30**, 1236–1240 (2014).
- 572 83. Conesa, A. et al. Blast2GO: a universal tool for annotation, visualization and
573 analysis in functional genomics research. *Bioinformatics* **21**, 3674–3676 (2005).
- 574 84. Li, L., Stoeckert, C. J., Jr. & Roos, D. S. OrthoMCL: identification of ortholog
575 groups for eukaryotic genomes. *Genome Res.* **13**, 2178–2189 (2003).
- 576 85. Li, H. et al. TreeFam: a curated database of phylogenetic trees of animal gene
577 families. *Nucleic Acids Res.* **34**, D572–D580 (2006).
- 578 86. Edgar, R. C. MUSCLE: multiple sequence alignment with high accuracy and high
579 throughput. *Nucleic Acids Res.* **32**, 1792–1797 (2004).
- 580 87. Capella-Gutierrez, S., Silla-Martinez, J.M. & Gabaldon, T. trimAl: a tool for

- 581 automated alignment trimming in large-scale phylogenetic analyses.
582 *Bioinformatics* **25**, 1972–1973 (2009).
- 583 88. Guindon, S., Delsuc, F., Dufayard, J. F. & Gascuel, O. Gascuel, Estimating
584 maximum likelihood phylogenies with PhyML. *Methods Mol. Biol.* **537**, 113–137
585 (2009).
- 586 89. Yang, Z. PAML 4: phylogenetic analysis by maximum likelihood. *Mol. Biol.*
587 *Evol.* **24**, 1586–1591 (2007).
- 588 90. De Bie, T., Cristianini, N., Demuth, J. P. & Hahn, M. W. CAFE: a computational
589 tool for the study of gene family evolution. *Bioinformatics* **22**, 1269–1271 (2006).
- 590 91. Tang, H. et al. Unraveling ancient hexaploidy through multiply-aligned
591 angiosperm gene maps. *Genome Res.* **18**, 1944–1954 (2008).
- 592 92. Schwartz, S. et al. Human-mouse alignments with BLASTZ. *Genome Res.* **13**,
593 103–107 (2003).
- 594 93. Bailey, J. A., Yavor, A. M., Massa, H. F., Trask, B. J. & Eichler, E. E. Segmental
595 duplications: organization and impact within the current human genome project
596 assembly. *Genome Res.* **11**, 1005–1017 (2001).
- 597 94. Birney, E., Clamp, M. & Durbin, R. GeneWise and Genomewise. *Genome Res.*
598 **14**, 988–995 (2004).
- 599 95. Ruan, J., Li, H., Chen, Z. & Coghlan, A. TreeFam: 2008 Update. *Nucleic Acids*
600 *Res.* **36**, D735–D740 (2008).
- 601 96. Tholl, D. et al. Practical approaches to plant volatile analysis. *Plant J.* **45**, 540–
602 560 (2006).

- 603 97. Wen, B., Mei, Z., Zeng, C. & Liu, S. metaX: a flexible and comprehensive
604 software for processing metabolomics data. *BMC Bioinformatics* **18**, 183 (2017).
- 605 98. Wen, P. et al. The sex pheromone of a globally invasive honey bee predator, the
606 Asian eusocial hornet, *Vespa velutina*. *Sci. Rep.* **7**, 12956 (2017).
- 607 99. Chen, Y., Chen, Y., Shi, C. & Huang, Z. et al. SOAPnuke: a MapReduce
608 acceleration-supported software for integrated quality control and preprocessing
609 of high-throughput sequencing data. *Gigascience* **7**, 1–6 (2018).
- 610 100. Langmead, B. & Salzberg, S. L. Fast gapped-read alignment with Bowtie 2. *Nat.*
611 *Methods* **9**, 357–359 (2012).
- 612 101. Li, B. & Dewey, C. N. RSEM: accurate transcript quantification from RNA-Seq
613 data with or without a reference genome. *BMC Bioinformatics* **12**, 323 (2011).
- 614 102. Tian, X., Chen, L., Wang, J., Qiao, J. & Zhang, W. Quantitative proteomics
615 reveals dynamic responses of *Synechocystis* sp. PCC 6803 to next-generation
616 biofuel butanol. *J. Proteomics* **78**, 326–345 (2013).
- 617 103. Wen, B., Zhou, R., Feng, Q., Wang, Q., Wang, J. & Liu, S. IQuant: an automated
618 pipeline for quantitative proteomics based upon isobaric tags. *Proteomics* **14**,
619 2280–2285 (2014).
- 620 104. Brosch, M., Yu, L., Hubbard, T. & Choudhary, J. Accurate and sensitive peptide
621 identification with Mascot Percolator. *J. Proteome Res.* **8**, 3176–3181 (2009).
- 622 105. Savitski, M. M., Wilhelm, M., Hahne, H., Kuster, B. & Bantscheff, M. A scalable
623 approach for protein false discovery rate estimation in large proteomic data sets.
624 *Mol. Cell. Proteomics* **14**, 2394–2404 (2015).

- 625 106.Cox, J. & Mann, M. MaxQuant enables high peptide identification rates,
626 individualized p.p.b.-range mass accuracies and proteome-wide protein
627 quantification. *Nat. Biotechnol.* **26**, 1367–1372 (2008).
- 628 107.Bruderer, R. et al. Extending the limits of quantitative proteome profiling with
629 data-independent acquisition and application to acetaminophen-treated three-
630 dimensional liver microtissues. *Mol. Cell. Proteomics* **14**, 1400–1410 (2015).
- 631 108.Dunn, W.B. et al. Procedures for large-scale metabolic profiling of serum and
632 plasma using gas chromatography and liquid chromatography coupled to mass
633 spectrometry. *Nat. Protoc.* **6**, 1060–1083 (2011).
- 634 109.Love, M. I., Huber, W. & Anders, S. Moderated estimation of fold change and
635 dispersion for RNA-seq data with DESeq2. *Genome Biol.* **15**, 550 (2014).
- 636 110.Choi, M. et al. MSstats: an R package for statistical analysis of quantitative mass
637 spectrometry-based proteomic experiments. *Bioinformatics* **30**, 2524–2526
638 (2014).
- 639 111.Wen, X.-L., Wen, P., Dahlsjö, C. A. L., Sillam-Dussès, D. & Šobotník, J.
640 Breaking the cipher: ant eavesdropping on the variational trail pheromone of its
641 termite prey. *Proc. R. Soc. B.* **284**, 20170121 (2017).
- 642 112.Bailey, T. L. & Elkan, C. Fitting a mixture model by expectation maximization to
643 discover motifs in biopolymers. *Proc. Int. Conf. Intell. Syst. Mol. Biol.* **2**, 28–36
644 (1994).
- 645 113.Langfelder, P. & Horvath, S. WGCNA: an R package for weighted correlation
646 network analysis. *BMC Bioinformatics* **9**, 559 (2008).

- 647 114. Yip, A. M. & Horvath, S. Gene network interconnectedness and the generalized
648 topological overlap measure. *BMC Bioinformatics* **8**, 22 (2007).
- 649 115. Langfelder, P., Zhang, B. & Horvath, S. Defining clusters from a hierarchical
650 cluster tree: the dynamic tree cut package for R. *Bioinformatics* **24**, 719–720
651 (2008).
- 652 116. Lescot, M. et al. PlantCARE, a database of plant cis-acting regulatory elements
653 and a portal to tools for in silico analysis of promoter sequences. *Nucleic Acids*
654 *Res.* **30**, 325–327 (2002).
- 655 117. Gendrel, A.V., Lippman, Z., Martienssen, R. & Colot V. Profiling histone
656 modification patterns in plants using genomic tiling microarrays. *Nat. Methods* **2**,
657 213–218 (2005).

658

659 **ACKNOWLEDGMENTS**

660 We thank Yong-Jin Wang, Qi-Chong Zhu, Qiong Sun, Qian-Ya Li, Jing-Wen Wang,
661 Tong-Lei Xu, Yue Chen, Fang-Lu Wei, Guo-Chun Shen, Xiu-Lian Wen and Li-Sha Li
662 for their kind helps in field experiments, Xiu-Lian Wen, Li-Sha Li and the Public
663 Technology Service Center of XTBG (CAS) for assisting active VOCs analysis, and
664 Xiu-Guang Mao, Pan-Yu Hua and Da-Yong Zhang for constructive suggestions in
665 data analysis. This work is supported by NSFC grants 31630008 and 31870356 (X.-
666 Y.C.), and 31870359 (G.W.); and a Talents 1000 Fellowship of Shaanxi Province
667 (D.W. D.). S.S. acknowledges departmental support from Harper Adams University.

668

669 **Author contributions**

670 X.-Y.C. and R.W. conceived and designed the study. R.W., Y.Yang., S.G.C., S.T.S.,
671 H.Y. and Z.Y. conducted the experiments and analyzed data. Y.J., Q.-F.L., H.Y., Y.Z.,
672 G.W., J.C., R.M., S.C., Y.C., D.W.D., H.-Q.L., M.L., Y.-Y.D., Y.-Y.L., X.T., P.W., J.-
673 J.Y., X.-T.Z., Q.G., J.-Y.Y., Y.Yin, K.J. and H.-M.Y. contributed to data acquisition
674 and data analyses. R.W., S.S., S.G.C., J.-Q.L., J.-Y.R., F.K., C.A.M, A.C., P.M.G, Y.-
675 Y.Z. and X.-Y.C. edited the manuscript. All authors contributed to writing the
676 manuscript.

677

678 **Competing interests**

679 The authors declare no competing interests.

680

681 **Additional information**

682 All supplemental figures and tables are included in supplementary information.

683

684 **Figure legends**

685 **Fig. 1 | Fig-pollinator mutualism between *F. pumila* var. *pumila* and *Wiebesia***

686 ***pumilae* and determination of the compound attracting *W. pumilae*. a, Life cycle**

687 **of *W. pumilae* based on four fig developmental stages (pre-receptive, receptive, post-**

688 **receptive and mature stages). This *Ficus* species is dioecious with figs on female trees**

689 **growing long-styled female florets (seed florets) that are not available for pollinator**

690 **oviposition. Therefore, female trees only produce seeds, while figs on functional male**

691 trees contain both male florets and short-styled female florets (feeder florets) that can
692 be used by female pollinators for oviposition to support the larvae of the pollinators.
693 At the receptive stage, adult female pollinators are attracted by host-specific VOCs
694 and enter figs only through ostiole (lined with bracts), either ovipositing into ovules of
695 feeder florets in functional male figs or pollinating seed florets inside female figs.
696 Pollinator larvae develop in induced galled ovules and both larvae and seeds grow
697 during the post-receptive stage. At the mature stage, after mating with adult males,
698 adult female pollinators leave their natal figs carrying pollen donated by mature male
699 florets and search for receptive figs and complete the cycle. **b**, Electrophysiological
700 responses of adult females of *W. pumilae* to the VOCs extracted from *F. pumila* var.
701 *pumila* figs at receptive stage using GC–EAD. Each curve represents the response of a
702 single female pollinator. **c**, Electrophysiological responses of adult female pollinators
703 to the synthesized standard of each tentative VOC compound (each
704 electroantennogram curve represents five overlapped replicates). **d**, Preference of
705 adult female pollinators to different tentative compounds using Y-tube olfactometer
706 tests (Supplementary Table 9).

707

708 **Fig. 2 | Molecular mechanisms of the specific host identification of *W. pumilae*.** **a**,

709 Numbers of genes in the four olfactory-related gene families (odorant-binding

710 proteins (OBPs), olfactory receptors (ORs), chemosensory proteins (CSPs) and

711 ionotropic receptor (IRs)) in different insect species. Significantly contracted families

712 (***) : $p < 0.001$) were shown for *W. pumilae* and *C. solmsi*, and species were ranked

713 according to their phylogeny (Supplementary Fig. 4b). **b**, Transcription and
714 translation of OBP genes of adult females of *W. pumilae* not contacting (as the
715 control) and contacting the VOCs emitted by *F. pumila* var. *pumila* figs at the
716 receptive stage (Supplementary Table 10). **c**, Motif analysis predicting the most likely
717 *W. pumilae* OBPs that can bind to decanal and nonanal (Supplementary Fig. 9). **d**, The
718 binding affinities (K_D) of the predicted OBPs to decanal and nonanal using surface
719 plasmon resonance (SPR) experiments (Supplementary Fig. 10 and Supplementary
720 Table 11). Lower K_D indicates higher binding affinity, and error bars represent
721 standard errors calculated by parameter estimation in steady state affinity model.

722

723 **Fig. 3 | Regulation of gene expression in attractant biosynthesis in figs of *F.***

724 *pumila* var. *pumila*. **a**, Pathways associated with biosynthesis of decanal and nonanal
725 (fatty acid biosynthesis (ko00061), elongation (ko00062) and metabolism (ko00071
726 and ko00592)). **b**, Fold changes of all PSDs and their transcriptomic expression
727 between receptive and pre-receptive stages in ostiolar types in proteomes
728 (Supplementary Table 12). ^{NS}: $p > 0.05$, ^{*}: $p < 0.05$, ^{**}: $p < 0.01$, ^{***}: $p < 0.001$. **c-e**, Results
729 of *in vitro* functional characterization of the four key genes in the biosynthesis of
730 decanal and nonanal. The peaks of synthesized standards and reaction products
731 (treatments with enzyme added for three replicates) were shown for each key gene.
732 Because there are two steps in the catalytic reaction of the two ACSLs, we showed the
733 ion intensity of both the intermediate product (hexadecanoyl-AMP) and the final
734 product (hexadecanoyl-CoA) separated by LC-MS. The reaction products of the

735 ALDH and the ADH (decanal and decanol) were identified using GC–MS. **f**,
736 Transcriptomic expression of genes in the co-expression module including two key
737 genes and the transcription factors predicted to regulate the expression of these two
738 key genes (Supplementary Tables 13 and 14). **g-h**, Results of ChIP–qPCRs (% input
739 and fold enrichment) showing the evidence that the predicted transcription factors can
740 bind to the promoter regions of *FpumACSL10* (FPUM_023966-RA) and
741 *FpumALDH1* (see Supplementary Tables 12 and 13). Error bars represent standard
742 errors of experimental results.

743

744 **Fig. 4 | Metabolic and genomic signature of antagonistic interaction between *F.***
745 ***pumila var. pumila* and *W. pumilae*.** **a**, Results of PLS-DA for terpenoids (triterpenes
746 and sesquiterpenes) and phenylpropanoids. Each oval indicates the 95% confidence
747 intervals of a sample group. **b**, Distribution of SMCDs across fates of female florets.
748 No SMSDs between feeder and seed florets and only three SMSDs (two
749 downregulated and one upregulated) between galled ovules and seeds were found in
750 the pathways related to plant chemical defenses (Supplementary Fig. 12). **c**, Largely
751 matched turnover of SMSDs in feeder floret-galled ovule and seed floret-seed
752 transitions (using Spearman’s rank correlation tests). **d**, Numbers of genes in
753 CYP450, CCE and GST gene families in different insect species. Significantly
754 contracted families (***: $p < 0.001$) were shown for *W. pumilae* and *C. solmsi*.

755 **Table 1 | Summary statistics for the assembly of *F. pumila var. pumila* and *W.***
 756 ***pumilae* genomes.**

757

Chromosome ID	<i>F. pumila var. pumila</i>		<i>W. pumilae</i>	
	No. of genes	Length (bp)	No. of genes	Length (bp)
Chr1	1,697	20,463,500	816	21,315,831
Chr2	1,871	21,202,951	2,076	59,985,216
Chr3	2,335	23,199,346	2,631	66,440,284
Chr4	2,412	23,721,380	2,225	54,409,331
Chr5	3,327	31,603,922	2,281	59,419,729
Chr6	1,649	20,816,579	2,263	55,968,755
Chr7	2,070	23,331,000		
Chr8	2,097	21,006,959		
Chr9	1,856	21,788,500		
Chr10	1,740	20,107,953		
Chr11	1,798	22,360,920		
Chr12	2,000	20,847,995		
Chr13	2,526	34,592,857		
Number of contigs	543		102	
Total length of contigs (Mb)	315.7		318.2	
Contig N50 (Mb)	2.3		10.9	
Anchored genome content (Mb)	304.8		317.5	
Anchored rate	96.6%		99.8%	
Scaffold N50 (Mb)	22.4		59.4	
Number of genes	28,187		12,316	

758

759 **Methods**

760 **Genome assembly and annotation.** Genomic DNA was extracted from leaves of a
761 female *F. pumila* var. *pumila* individual nearby Zhejiang Tiantong Forest Ecosystem
762 National Observation and Research Station (TINAS) (E 121°47', N 29°48'), Ningbo,
763 China, and from c. 500 adult female pollinators of *W. pumilae* emerged from five figs
764 on a functional male tree in South China Botanic Garden (SCBG) (E 113°11', N
765 23°11'), Guangzhou, China. Six pair-end and mate-pair libraries were prepared with
766 varying insert sizes (Supplementary Table 1) for sequencing on an Illumina Hiseq
767 4000 platform. We also carried out PacBio single-molecule real-time sequencing of
768 20kb SMRTbell libraries using a PacBio Sequel platform. Based on the Illumina pair-
769 end sequencing data, the genome sizes of both species were estimated by counting k-
770 mer frequency using Jellyfish version 2.1.3⁵².

771 *De novo* genome assembly was conducted using MECAT version 1.2⁵³. The
772 initial contig was polished twice based on raw PacBio data and then corrected twice
773 using Illumina paired-end reads with pilon version 1.22⁵⁴. Redundans version 0.13c⁵⁵
774 was used to exclude redundant contigs, and we removed contaminative sequences by
775 searching against the NCBI nucleotide sequences database
776 (<ftp://ftp.ncbi.nlm.nih.gov/blast/db/FASTA/>) using megablast⁵⁶ with e-value $\leq 1e^{-5}$.
777 Gap filling was implemented with PBJelly⁵⁷ after scaffolding based on Illumina mate-
778 pair reads using BESST version 2.2.7⁵⁸.

779 To further improve the quality of genome assembly of both species, we used
780 high-throughput chromatin conformation capture (Hi-C) technique to scaffold contigs
781 into pseudo-chromosomes. We constructed Hi-C libraries using the protocol described

782 by Belton et al.⁵⁹. Fresh leaves sampled from the same *F. pumila* var. *pumila*
783 individual used in above sequencing and adult female pollinators from SCBG were
784 cross-linked by 4% formaldehyde solution, followed by an overnight digestion with a
785 4-cutter restriction enzyme MboI (400 units) at 37°C, preparation DNA ends with
786 biotin-14-dCTP and blunt-end ligation of the cross-linked fragments. Then, the
787 proximal chromatin DNA was re-ligated by ligation enzyme, and the nuclear
788 complexes were reverse cross-linked by proteinase K. After that, we extracted and
789 purified DNA and removed biotin from non-ligated fragment ends using T4 DNA
790 polymerase. The following steps including end reparation, enrichment of biotin-
791 labeled Hi-C samples, and ligation by Illumina paired-end (PE) sequencing adapters,
792 and then the Hi-C library (insert size of 350 bp) was amplified by PCR and sequenced
793 on an Illumina NovaSeq 6000 platform. High quality data checked by HiC-Pro⁶⁰ were
794 mapped to genome using BWA, with extraction of uniquely mapped reads for pseudo-
795 chromosome clustering and assembly using Juicer⁶¹ and 3D-DNA⁶².

796 Following genome assembly, we assessed completeness using BUSCO version
797 3.0.3⁶³ and Iso-Seq full-length transcripts. The high-quality full-length transcripts
798 were mapped to genome assemblies using GMAP version 2014-12-21⁶⁴, setting a
799 cutoff of aligned coverage at 0.85 and aligned identity at 0.9. The quality of genome
800 assembly was further tested by mapping Illumina paired-end reads to the genome
801 assemblies using BWA with the depth of coverage calculated using BamDeal version
802 0.19 (<https://github.com/BGI-shenzhen/BamDeal/>). For each species, Iso-Seq
803 sequencing was performed using a PacBio Sequel platform, based on two SMRTbell

804 libraries with insert sizes of 0 - 5kb and 4.5kb - 10kb established by full-length
805 complementary DNA (cDNA). We used fresh leaves, young stems from fertile and
806 sterile branchlets and figs at different developmental stages for the plant, and adult
807 males and females for the pollinator.

808 Genome annotation includes repeat identification (including tandem repeats
809 (TRs) and transposable elements (TEs)), annotation of non-coding RNAs (ncRNA)
810 and gene prediction and annotation. When annotating repeat sequences, TRs were
811 identified using Tandem Repeats Finder (TRF) version 4.07⁶⁵, and TEs were searched
812 against Repbase 21.01⁶⁶ and the transposable element protein database using
813 RepeatMasker version 4.0.6 (<http://www.repeatmasker.org/>) and RepeatProteinMask
814 in RepeatMasker. LTR_Finder⁶⁷, PILER⁶⁸ and RepeatScout⁶⁹ were used to create a *de*
815 *novo* TE library, and the combined non-redundant library was classified by running
816 RepeatMasker again.

817 To annotate ncRNAs, tRNAscan-SE version 1.3.1⁷⁰ was used to identify tRNA
818 and their secondary structures. While small nuclear RNA (snRNA) and microRNAs
819 (miRNAs) were searched for using INFERNAL version 1.1.1⁷¹ in the Rfam database
820 version 12.0⁷², followed by the detection of rRNAs by aligning with plant or
821 invertebrate rRNA sequences using BLASTN (E-value $\leq 1e^{-5}$).

822 Gene model prediction was conducted using the MAKER pipeline version
823 2.31.10⁷³. The Iso-Seq full-length transcripts, RNA-seq transcripts (assembled using
824 Hisat2 version 2.0.1⁷⁴ and StringTie version 1.3.3⁷⁵), the protein sequences of related
825 species and protein sequences from Swiss-Prot database (<https://www.uniprot.org>)

826 were included in the analysis. Ab-initio gene prediction was performed with the gene
827 predictors SNAP⁷⁶ and AUGUSTUS⁷⁷. The MAKER pipeline was run for two (for the
828 plant) and three (for the pollinator) iterations for training and the final trained hidden
829 Markov model (HMM) was used for annotation. JBrowse version 1.12.3⁷⁸ was used to
830 examine the gene models following each iteration. The gene models with the presence
831 of a PFAM domain or with AED ≤ 0.6 for *W. pumilae* and AED < 1 for *F. pumila* var.
832 *pumila* were retained. BUSCO was used to evaluate the completeness of gene
833 annotation for both genomes.

834 After determining gene models, functions of protein-coding genes were annotated
835 using DIAMOND version 0.8.23⁷⁹ by aligning them to NCBI NR database, Swiss-
836 Prot⁸⁰ and KEGG⁸¹ databases. Motifs and domains in protein sequences were
837 annotated using InterProScan version 5.16-55.0⁸² via searching public databases.
838 Gene Ontology terms for each gene were assigned using Blast2GO version 3.3⁸³.

839 **Comparative genomics.** To analyze the evolutionary characters of our studied
840 genomes, we first carried out gene family clustering. The genome and annotation data
841 of 13 other angiosperm species and 11 other arthropod species were downloaded
842 (Supplementary Table 6). The gene models with open reading frames shorter than
843 90bp were removed, and only the longest transcript was chosen to represent each
844 gene. Gene family clustering was performed using OrthoMCL version 10-148⁸⁴ for
845 the plant and TreeFam pipeline version 0.5.1⁸⁵ for the pollinator.

846 We then determined the phylogenetic relationships among the plants and among
847 the insects in the species pools used in gene family clustering. Corresponding coding

848 sequences (CDSs) were aligned based on the protein sequences of all single-copy
849 orthologs using MUSCLE version 3.8.31⁸⁶, and codon position 2 of aligned CDSs
850 were concatenated into a super gene using an in-house Perl script with a filtration of
851 ambiguously aligned positions using trimAI version 1.4.1⁸⁷. After that, phylogenetic
852 trees were reconstructed using PhyML version 3.0⁸⁸ using a GTR substitution model
853 with a gamma distribution and 100 bootstrap replicates. PAML version 4.9⁸⁹ was used
854 to estimate divergence time, setting 10,000 MCMC generations with a sampling
855 frequency of 5,000 and a burn-in of 5,000,000 iterations. Overall substitution rate was
856 assessed using BASEML setting a REV substitution model.

857 Gene family expansion and contraction was analyzed using CAFE version 2.1⁹⁰,
858 which employed a stochastic birth-and-death process to model the evolution of gene
859 family sizes over a phylogeny. The birth-and-death parameter (λ) was estimated using
860 10,000 Monte Carlo random samples. We then used family-wise method to
861 statistically test if a gene family experienced significant expansion/contraction, and
862 gene families with conditional P-values less than 0.05 were considered to have
863 accelerated rates of gains and losses.

864 We then tested whether the genomes of *F. pumila* var. *pumila* experienced whole
865 genome duplication (WGD). Syntenic blocks were identified using MCscan version
866 0.8⁹¹, and the rate of transversions on fourfold degenerate synonymous sites (4DTv)
867 was calculated using the HKY substitution model to uncover potential speciation or
868 WGD events occurring in evolutionary history of the plant. For *W. pumilae*, we tested
869 for genomic segmental duplications (SDs). The self-alignment was performed using

870 BLASTZ version 1.02⁹², and a non-redundant set of SDs was obtained using WGAC
871 version 1.3⁹³.

872 **Annotation of specific gene families and analysis of their evolution.** To test
873 whether the contraction specific gene families in *W. pumilae*, *E. verticillata* and *C.*
874 *solmsi* contributes to the wasps' host-specificity and detoxification ability, we
875 conducted a detailed annotation in chemosensory gene families (OBPs, CSPs, ORs
876 and IRs) and detoxification gene families including CYP450s, GSTs and CCEs. The
877 homologous genes of *N. vitripennis*, *Apis mellifera* and *Drosophila melanogaster*
878 were used as queries to search the genome assembly of *W. pumilae* using TBLASTN
879 at a criterion of E-value $\leq 1e^{-5}$, and gene structures of identified genes were predicted
880 using GeneWise version 2.4.1⁹⁴ with pseudogenes masked. We repeated this process
881 iteratively until no more genes were detected. Additional genes from the MAKER
882 annotation were also included if they included corresponding InterPro domains. All
883 gene structures were manually checked and corrected if necessary, on the basis of full-
884 length transcripts, RNA-seq transcripts and homologous proteins in JBrowse. We used
885 Binomial Distribution One-tailed test to examine gene family expansion/contraction
886 among the compared species without considering their evolutionary relationships.

887 To reveal the evolutionary history of OBP, CYP450, CCE and GST gene families,
888 syntenic blocks were identified across the genomes of the three pollinating wasp
889 species and *N. vitripennis* using MCscan (<https://github.com/tanghaibao/jcvi/wiki>
890 /MCscan-(Python-version)). We then constructed neighbor-joining phylogenetic trees
891 to verify homologous genes among these insect species, using TreeBeST version

892 1.9.2⁹⁵ using a JTT model and 1000 bootstraps.

893 **VOC collection and component analysis.** To reveal the composition of volatile
894 organic compounds (VOCs) emitted by figs of *F. pumila* var. *pumila* at different
895 developmental stages, we collected VOCs from figs at both pre-receptive and
896 receptive stages (Fig. 1a) in spring 2018 using dynamic headspace sampling (DHS)
897 techniques⁹⁶. After a careful search, we chose ten mature *F. pumila* var. *pumila* trees
898 comprising five females and five functional males (Supplementary Table 8) nearby
899 TINAS, within the natural range of the plant. Three figs were labeled on each selected
900 individual. At either fig developmental stage (from early to middle April for pre-
901 receptive stage and late April for receptive stage), we extracted the VOCs emitted by
902 each labeled fig into an activated porapak adsorption tube (150 mg) during 8:00-11:00
903 am, using a protocol identical to Tholl et al. (2006)⁹⁶. Each adsorption tube was then
904 eluted three times using 300 μ l n-hexane and stored at -20 °C.

905 VOCs emitted by figs were then separated and identified using a coupled Gas
906 Chromatography-Mass Spectrometry (GC-MS) system (HP 7890A-5975C, Agilent,
907 US)⁹⁷. For each sample, 1.8 μ l of eluate VOC extract, concentrated using nitrogen,
908 was injected in split mode with a split ratio of 10 : 1 at 250 °C. Helium (1 mL/min)
909 was used as carrier gas in a HP-5ms (30 m \times 250 μ m \times 0.25 μ m, Agilent, US) GC
910 column. We set the oven ramp at 40°C for 1 min, and then 3 °C/min to 140 °C for 1
911 min, followed by 5 °C/min to 230 °C for 3 mins. Ionization was conducted by
912 electron impact (70 eV, source temperature 230 °C). The MS quadrupole was heated
913 to 150 °C, with the scanned mass range setting as from 40 to 550 m/z. Compound

914 identification was implemented by matching the mass spectra with NIST 08 MS
915 libraries. We then calculated the relative proportions of all compounds emitted by figs
916 at each developmental stage.

917 To evaluate the difference in the concentration of decanal between ostiolar tissues
918 and female florets, we sampled figs at receptive stages from three female and three
919 functional male individuals and identified the composition of VOCs emitted from
920 these two types of tissues using the same approach mentioned above. The decanal
921 concentration in each type of tissues in a plant individual was quantified by
922 comparing its peak area with the internal standard (decyl acetate).

923 **Electrophysiological responses of pollinating wasps.** To narrow the range of
924 candidate VOCs attracting *W. pumilae*, we tested the electrophysiological responses of
925 the pollinators to the collected VOCs, using gas chromatography-electroantennogram
926 detection (GC–EAD). We used a system coupling a custom-made EAG⁹⁸ with a GC
927 (Trace GC 2000, Thermo Finnigan, US). We injected 1.8 µl of concentrated VOC
928 extract eluate into the GC to separate different compounds. The GC conditions were
929 identical to those used for the GC–MS component analysis, except that the oven ramp
930 was set to 50 °C for 2 mins, and then to 10 °C/min up to 280 °C for 1 min. After GC–
931 FID (flame ionization detector) quantification, outflow from the GC column was
932 delivered to the EAG as the stimulus through a custom, 40 cm long heated (at 250 °C)
933 transfer line with a clean, wet, and static-free airflow. The stimulus was then puffed to
934 the antenna of an adult female pollinator (collected from figs in TINAS) fixed onto
935 the EAG with both ends of the antennae connected with prepared glass electrodes

936 linking the probes of EAG to the potentiometric amplifiers.

937 This experiment was repeated 5 times (i.e. antennae of 5 adult female
938 pollinators), and the EAD signal was recorded using a HP 34465A digital multimeter
939 (Keysight, US). Both EAD and FID signal data were aligned to verify the tentative
940 compounds stimulating the adult female pollinator, using the software IO Libraries
941 Suite 16 (Agilent, US) and BenchVue (Keysight, US). These tentative effective
942 compounds were identified by matching the chromatographs with the results of
943 component analysis using GC–MS.

944 We further tested the electrophysiological response of adult female pollinators
945 (collected from figs in SCBG) to the synthesized standard of each tentative compound
946 (TIC, JPN; TRC, CAN; Sigma-Aldrich, US), following the same procedures as above.
947 A compound was determined as truly effective only when it was confirmed by the
948 experiments using both eluate of VOC extracts and synthesized standard.

949 **Behavioral preference of pollinating wasps.** To test the behavioral preference of *W.*
950 *pumilae* to different tentative effective VOCs, we used a Y-tube olfactometer (stem 8
951 cm, arms 9 cm, at an angle of 55°, internal diameter of 1.5 cm) following the methods
952 described by Wang et al.¹⁹. We placed the synthesized standard of each tentative
953 effective VOC in the glass container, connecting one arm of the olfactometer to this
954 treatment of n-hexane and blends of putative stimuli compounds and the other arm to
955 the controls (only n-hexane) (Supplementary Table 9). VOCs were passed from both
956 arms to the stem through equal flow rates of cleaned and humidified airflow created
957 by an air pump system with an activated charcoal filter and distilled water. To avoid

958 visual distractions to the pollinators, we placed the olfactometer in the center of a
959 white table illuminated using three 40-W cool white fluorescent tubes above the arms.

960 Each healthy adult female pollinator (collected from figs in SCBG) was tested
961 independently with an observation for 5 mins in the olfactometer, and its behavior was
962 assigned to one of the three choices: (1) towards the treatment (the insect went 1 cm
963 past the Y junction (decision line) and stayed there more than 1 min); (2) towards the
964 control; and (3) no choice (the insect did not reach the decision line within 5 mins).

965 For each treatment-control combination, we repeated this experiment 50 times (i.e. 50
966 adult female pollinators) and compared the proportions of different choices (towards
967 the treatment and towards the control) using GLMs assuming binomial distribution of
968 residuals to examine the preference of *W. pumilae*.

969 **Sample collection for comparative transcriptome, proteome and metabolome.** To
970 reveal the molecular mechanisms forming the specific pollinator-host identification
971 based on both transcriptomic and proteomic data, in spring 2017, after collecting
972 several pre-receptive and receptive figs from the ten mature individuals of the plants
973 used in VOCs collection (Supplementary Table 7), we dissected each sampled fig to
974 gather ostiolar tissues with bracts. The total sample size therefore was 20 for the plant.
975 In spring 2018, we sampled at least 5 figs at the mature stage from each of the five
976 functional male mature individuals used for VOC collection (Supplementary Table 7).
977 Each sampled mature fig was dissected into halves in a Teflon bag, and then each half
978 was rapidly moved into a Teflon bag containing only clean air filtered by activated
979 charcoal (as a control) or clean air and a receptive fig (as a treatment), to test whether

980 differential expression occurred in some chemosensory genes when adult females
981 were exposed to attractive VOCs. We then collected all adult females of *W. pumilae*
982 emerging from the sampled figs according to the identity of functional male trees (a
983 total of 10 samples with at least 100 adult female wasps in each sample). All sampled
984 fig tissues and adult female pollinators were first stored in liquid nitrogen for 72 hours
985 and then moved into a refrigerator at -80 °C.

986 To unravel how pollinator larvae adapt to the environments inside galled ovules
987 using metabolomes, we sampled several receptive and post-receptive figs from the ten
988 plant individuals (Supplementary Table 7) and collected ostiolar tissues (20 samples),
989 female florets (10 samples), galled ovules (5 samples) and seeds (5 samples) in spring
990 2020. For clearly distinguishing galled ovules and seeds from the female florets that
991 were neither pollinated nor utilized by pollinators, the post-receptive figs were
992 sampled four weeks after the entrance of adult female pollinators.

993 **RNA-seq for *F. pumila* var. *pumila* and *W. pumilae*.** After generating PCR-based
994 libraries and sequencing on a BGISEQ500 platform (BGI, CHN), low quality reads
995 were filtered using SOAPnuke version 1.5.6⁹⁹. The acquired clean reads were then
996 mapped to the genome assemblies of our studied species using Bowtie version 2.2.5¹⁰⁰
997 and gene expression were quantified by RSEM version 1.2.12¹⁰¹.

998 **Quantitative proteomes for *F. pumila* var. *pumila* and *W. pumilae*.** We identified
999 and quantified proteins for ostiolar tissues (sampled in 2017) using iTRAQ (isobaric
1000 tags for relative and absolute quantitation)-based method. The strategy of quantifying

1001 proteomes was conducted according to the methods described by Tian et al. (2013)¹⁰².
1002 After total protein extraction, peptide labeling was performed using an iTRAQ
1003 Reagent 8-plex Kit according to the manufacturer's protocol. Extraction was followed
1004 by peptide fractionation, and the peptides separated from LC-20AD nano-HPLC
1005 (Shimadzu, JPN) were transferred into the tandem mass spectrometry Q EXACTIVE
1006 (MS/MS) (Thermo Fisher Scientific, US) for data-dependent acquisition (DDA)
1007 detection. After converting the raw MS/MS data into MGF format using Proteome
1008 Discoverer version 1.2 (Thermo Fisher Scientific, US), the exported data in MGF
1009 format were searched using Mascot version 2.3 (Matrix Science, US) against the
1010 protein-coding sequences from our gene prediction. Quantification of proteins was
1011 achieved using IQuant¹⁰³, which uses the Mascot Percolator algorithm¹⁰⁴ to improve
1012 the results of peptide identification and the principle of parsimony to assemble
1013 proteomes. All the proteins with a false discovery rate (FDR)¹⁰⁵ of less than 1% were
1014 retained for further analyses.

1015 We used a DIA (data independent acquisition) approach to identify and quantify
1016 proteins in adult female pollinators (collected in 2018). Procedures identical to
1017 iTRAQ were first performed on the total protein extraction, peptide fractionation and
1018 peptides separation. Then, to create reference spectra for DIA, we first conducted
1019 DDA on a Q-EXACTIVE HF mass spectrometer (Thermo Fisher Scientific, US)
1020 coupled with an Ultimate 3000 RSLCnano system (Thermo Fisher Scientific, US)
1021 after a further peptide separation on an in-house packed nano-LC column (150 μm \times
1022 30 cm, 1.8 μm , 100 \AA). Then, using the same instruments, DIA was performed

1023 following a brief procedure that consisted of a survey scan at 120,000 resolution from
1024 400 to 1,250 m/z (MIT 50 ms), followed by scanning in DIA isolation windows
1025 setting 17 m/z with loop count 50 at 30,000 resolution (automatic gain control target
1026 3×10^6 and auto MIT). The DDA spectra were identified by searching against the
1027 database of protein-coding sequences using the MaxQuant version 1.5.3.30¹⁰⁶ (Cox
1028 and Mann, 2008) at the FDR level of 1% with the minimum peptide length of 7.
1029 Based on the spectrogram database of DDA spectra, peptides and proteins in DIA data
1030 were identified and quantified using Spectronaut¹⁰⁷, employing the mProphet
1031 approach and setting iRT for retention time prediction. A target-decoy model was used
1032 to verify the quantification results at an FDR level of 1%.

1033 **Measurement of metabolomes of different types of tissues.** Chromatographic
1034 separation of metabolites was performed using an Ultra-Performance Liquid
1035 Chromatography (UPLC) System (Waters, UK), with an ACQUITY UPLC HSS T3
1036 column (100mm*2.1mm, 1.8 μ m) (Waters, UK) being used for the reversed phase
1037 separation and setting oven temperature at 50° C and flow rate of 0.4 ml/min. After
1038 separation, gradient elution was conducted as following procedure: 0~2 min, 100%
1039 mobile phase A (water + 0.1% formic acid); 2~11 min, 0% to 100% mobile phase B
1040 (acetonitrile + 0.1% formic acid); 11~13 min, 100% B; 13~15 min, 0% to 100% A.
1041 The injection volume for each sample was 10 μ l. Then, the eluted metabolites were
1042 identified in both positive and negative ion modes using a high-resolution tandem
1043 mass spectrometer Xevo G2 XS QTOF (Waters, UK). The capillary and sampling
1044 cone voltages were set at 3.0 kV and 40.0 V for positive ion mode and at 2.0 kV and

1045 40.0 V for negative ion mode. Mass spectrometry data were acquired in Centroid
1046 MSE mode, setting the TOF mass range from 50 to 1200 Da and the scan time of 0.2
1047 s. For MS/MS detection, all precursors were fragmented at 20-40 eV with the scan
1048 time of 0.2 s. A quality control (QC) sample (pooling all samples together) was used
1049 after every 10 samples. Peak alignment, peak picking and quantitation of each
1050 metabolite were performed using Progenesis QI version 2.2, and the quality control
1051 based on LOESS signal correction¹⁰⁸ was conducted using QC samples.

1052 **Comparative transcriptome, proteome and metabolome analysis.** We carried out
1053 differential expression/concentration analysis for transcriptomes, proteomes and
1054 metabolomes, to detect the key genes contributing to the attractant-induced host
1055 specificity and the chemical cues for the adaptation of pollinator larvae to plant
1056 chemical defenses.

1057 For transcriptomes, differential expression was tested in ostiolar tissues between
1058 the pre-receptive and the receptive stage. For the pollinator, differential expression
1059 was conducted between contacting attractive VOC(s) vs. not contacting and between
1060 adults and larvae. We performed comparisons using DEseq2 version 1.4.5¹⁰⁹ based on
1061 negative binomial distributions. *P*-values were corrected using a Benjamini-Hochberg
1062 (BH) method for multiple tests. The differentially expressed genes (DEGs) with a fold
1063 change ≥ 2 and an adjusted *p*-value ≤ 0.05 were considered as statistically significant.

1064 For proteomes, we tested the proteins with significant difference in quantity
1065 (PSDs) in ostiolar tissues between the pre-receptive and the receptive stages and
1066 between sexes at each stage using IQuant, and PSDs were defined as fold changes in

1067 protein abundance ≥ 1.2 and Q-value ≤ 0.05 . In adult female pollinators, PSDs were
1068 analyzed using MSstats¹¹⁰ at criteria of fold changes ≥ 2 and Q-value ≤ 0.05 .

1069 For metabolomes, to examine whether there were significant differences in
1070 profile of secondary metabolites associated with chemical defenses (SMCDs) between
1071 different types of tissues and between the receptive and the post-receptive stages, we
1072 first carried out enrichment analysis to enrich all relevant secondary metabolites into
1073 the pathways associated with plant chemical defenses and then clustered all samples
1074 into different categories using PLS-DA model in metaX¹¹¹. Data were log₂-
1075 transformed and scaled by Pareto scaling. Secondary metabolites with significant
1076 difference in quantity (SMSDs) were defined as VIP (variable importance for the
1077 projection calculated based on the first two axes from PLS-DA model) ≥ 1 , fold
1078 change ≥ 1.2 or ≤ 0.83 and Q-value ≤ 0.05 . In addition, we performed PLS-DA model
1079 to test the difference in the entire profile of secondary metabolites between different
1080 types of tissues and between different fig developmental stages.

1081 **Motif analysis.** We conducted motif analysis to check whether the OBPs in the same
1082 syntenic blocks among the three pollinating wasp species have similar motif structure
1083 using MEME Suite 5.0.4¹¹². Motifs with E-value ≤ 0.05 were used for inter-specific
1084 comparisons. To predict the most likely OBPs related to the identification of specific
1085 attractant and repellent, we created a dataset consisting of all OBPs in *W. pumilae* and
1086 the specific OBPs that had been verified to bind to decanal and nonanal in
1087 *Adelphocoris lineolatus*³³ and *Culex quinquefasciatus*³⁴ as references, and performed
1088 motif analysis.

1089 ***In vitro* functional characterization of key genes.** The full-length of open reading
1090 frame (ORF) of the four key genes (for the plant) and of the two OBPs (for the
1091 pollinator) (Supplementary Table 17) was confirmed by RT-PCR and was then cloned
1092 into pET-28a (MilliporeSigma, US). After checking sequences by Sanger sequencing,
1093 these genes were expressed in *E. coli* strains BL21 (DE3) and Rosetta (DE3). The
1094 recombinant proteins produced were purified (purity > 90%) using modified nickel-
1095 nitrilotriacetic acid agarose (Thermo Fisher Scientific, US).

1096 We measured the affinities of the two OBPs to different substrates using surface
1097 plasmon resonance (SPR) on a Biacore T200 system (GE Healthcare). OBPs were
1098 reconstituted in sterile PBS and were diluted in 10mM sodium acetate trihydrate (pH
1099 = 4.5) to the concentration of 20ug/ml. Then, each OBP was immobilized by the
1100 amine coupling method on a CM5 sensor chip according to the manufacturer's
1101 protocol (GE Healthcare). Analytes (decanal and nonanal) were diluted in running
1102 buffer (5% DMSO-PBS-P) to the concentration ranging from 0 to 1000 μ M and were
1103 injected through channels at a flow rate of 20 μ l/min. Using BIAevaluation (GE
1104 Healthcare), both steady state affinity model and 1:1 binding model were performed
1105 to quantify the binding affinity (K_D).

1106 For enzyme activity assays of the four key genes of the plant, we used the
1107 reaction system (500 μ l) mainly composed of 50 mM Tris-HCl (pH 7.4), 0.4~1.0 mM
1108 substrate(s) (Supplementary Table 17), 2M dimethyl sulfoxide (for the ADH and the
1109 ALDH)/10% triton X-100 (for the two ASCLs), and 10 μ l of purified protein (0.2
1110 mg/ml). After 60 min of incubation at room temperature, we collected the reaction

1111 products by headspace solid-phase microextraction for the ALDH and the ADH
1112 (which were analyzed by GC–MS) and by extraction using diethyl ether for the two
1113 ACSLs (which were analyzed by LC–MS). These experiments were repeated for three
1114 time. In addition, three replications of negative controls (only adding the substrates and
1115 bovine serum albumin) were conducted, and no reaction products were detected.

1116 **Cis-element detection and co-expression network analysis.** To test the regulatory
1117 mechanisms in the biosynthesis of attractant and repellent emitted by figs of *F. pumila*
1118 var. *pumila*, we first scanned the binding motifs present in the 2-kb promoter
1119 sequences upstream of key plant genes using PlantCARE¹¹⁶. Then, weighted
1120 undirected co-expression networks were conducted using the R package WGCNA¹¹³
1121 with a soft thresholding power of 8. Modules containing genes with correlated
1122 expression patterns were identified by gene clustering based on the topological
1123 overlap matrix¹¹⁴ and by cutting the resulting dendrogram using the cutreeDynamic
1124 approach in the R package The Dynamic Tree Cut¹¹⁵. Genes with kME values larger
1125 than 0.95 were selected as hub genes. We checked whether some modules containing
1126 both some key plant genes and the transcription factors predicted to bind to them. This
1127 allowed us to uncover the likely regulatory mechanisms.

1128 **ChIP-qPCR.** The open reading frame of each of the four transcription factors
1129 (*FpumHD-ZIP1*, *FpumHD-ZIP2*, *FpumbZIP1* and *FpumbHLH1* (Supplementary
1130 Table 13)) was cloned into the pET-28a to generate the fusion plasmid encoding the 6
1131 His-tagged fusion protein. This plasmid was transformed into *E. coli* strain Rosetta

1132 (DE3), which were cultured and induced by 0.8 mM isopropyl- β -D-thiogalactoside
1133 (IPTG) at 37 °C. The induced cells were then sonicated for supernatant collection, and
1134 the purified recombinant proteins were obtained using a His-tag Protein Purification
1135 Kit (Beyotime Biotechnology, CHN). The purified proteins were used to immunize
1136 rabbits for 52 days to acquire polyclonal antibody (ABclonal Biotechnology, CHN).
1137 We successfully obtained the qualified antibodies for all the four transcription factors
1138 for ChIP-qPCR experiments.

1139 ChIP-qPCRs were then conducted for the two transcription factors with qualified
1140 antibodies to examine if it can bind the putative target genes by model prediction. The
1141 ChIP assay was performed based on the protocols described in Gendrel et al.,
1142 (2005)¹¹⁷. Approximately 3.0 g ostiolar tissues from figs at receptive stages were
1143 treated using 1% formaldehyde to crosslink and fix the DNA-protein complexes. The
1144 cells of sampled tissues were lysed, and each antibody was used to immunoprecipitate
1145 the antigen transcription factor with its binding DNA fragments. The DNA in the ChIP
1146 products was applied in qPCR with primer pairs designed for the promoters of
1147 putative target genes in a QuantStudio™ 5 real-time PCR detection system (Thermo
1148 Fisher Scientific, US). Each qPCR reaction was performed in triplicates, and the cycle
1149 thresholds (Cts values) of ChIP products were compared with those of input samples
1150 and negative controls (only using IgG) for calculating % input and fold enrichment (%
1151 input (ChIP)/ % input (negative control)). We failed to obtain the Ct values for
1152 negative controls by the end of 35 qPCR cycles, and we therefore used the Ct value of
1153 35 for each negative control when calculating % input and fold enrichment.

1154

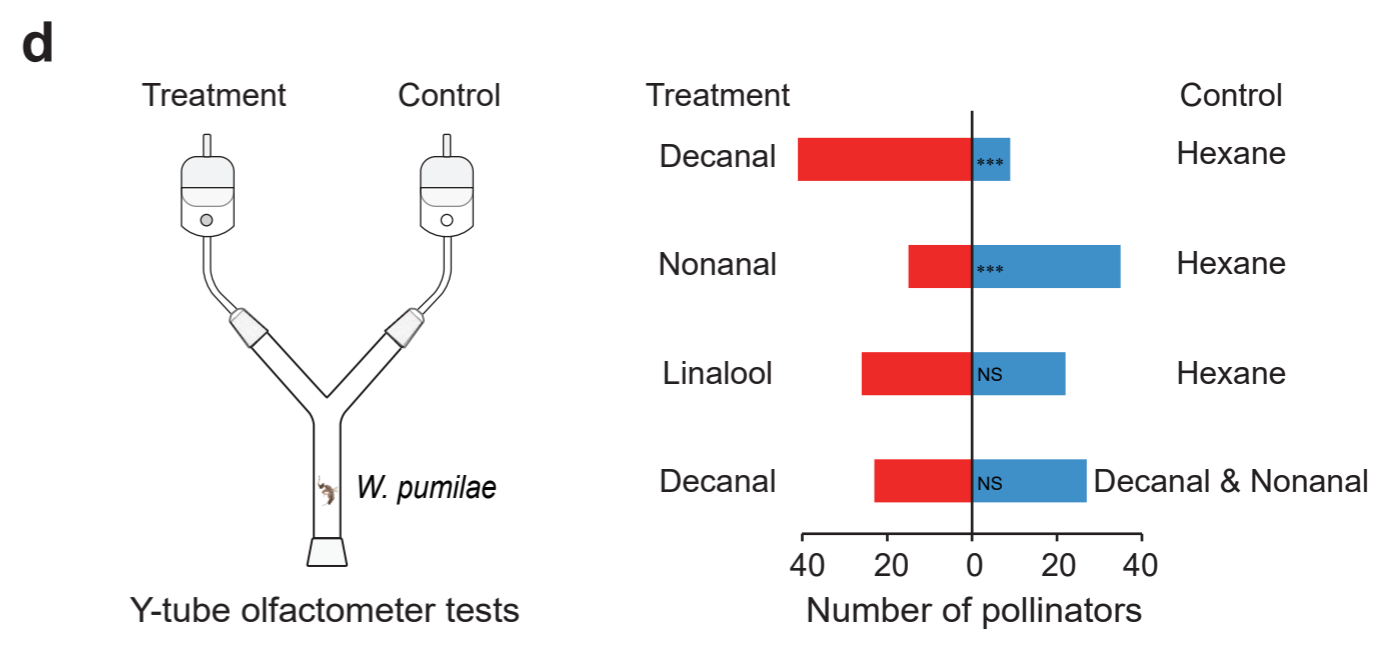
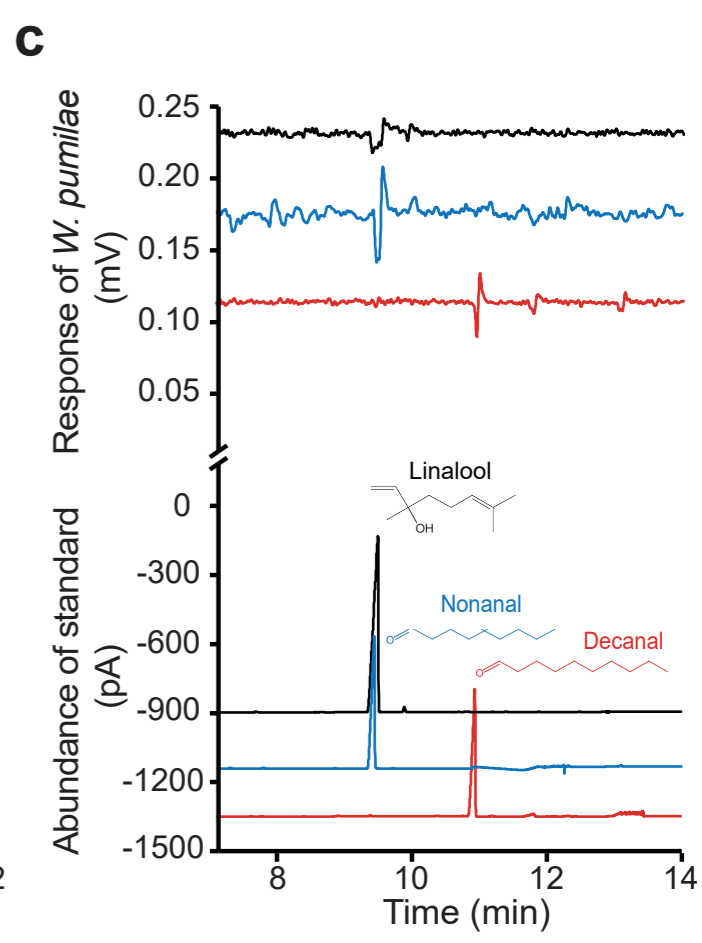
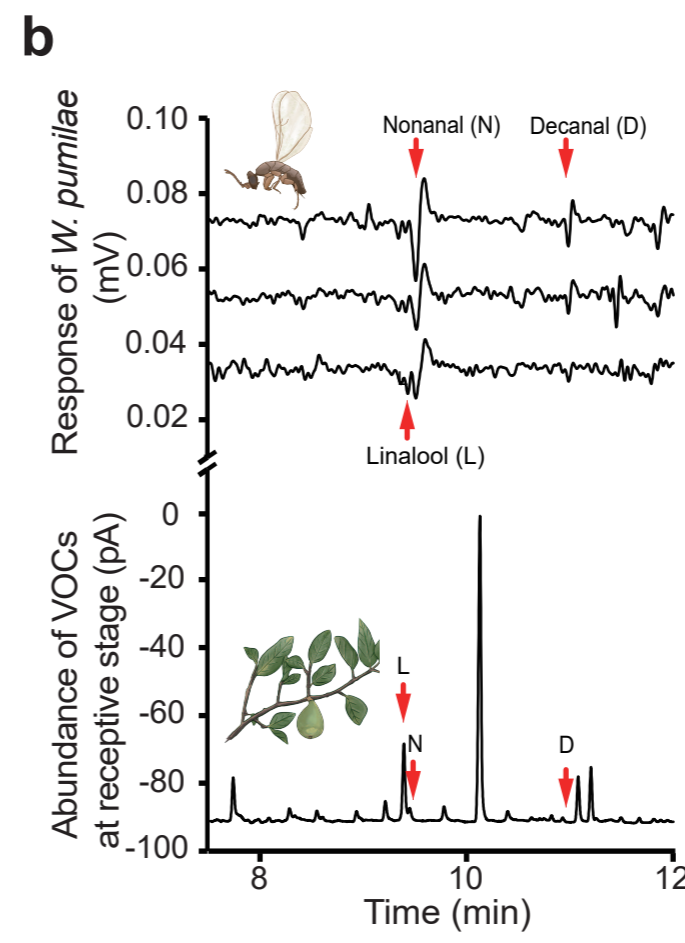
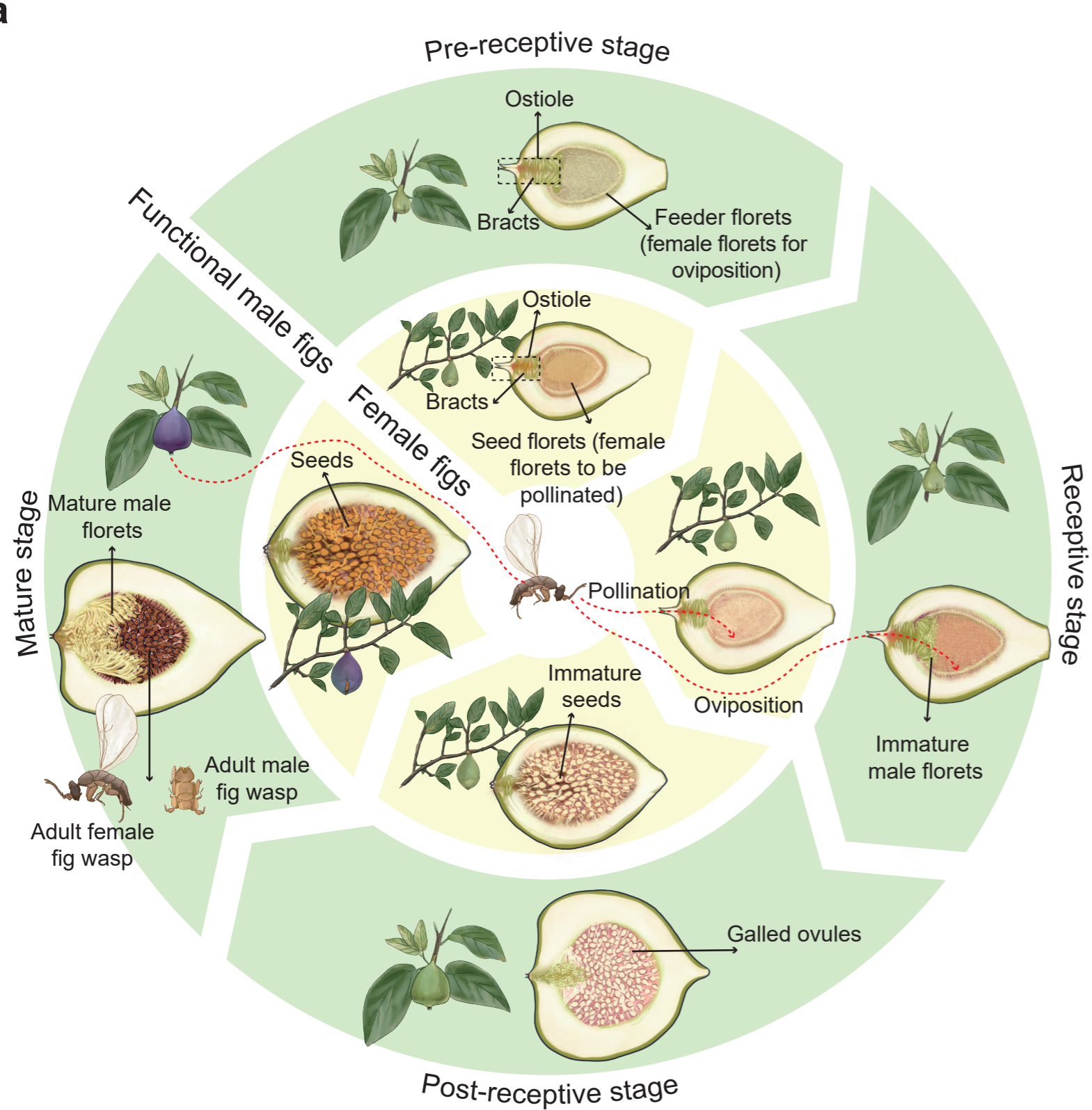
1155 **Data availability**

1156 The data that support the findings of this study have been deposited in the CNSA
1157 (<https://db.cngb.org/cnsa/>) of CNGBdb with accession code CNP0000674.

1158

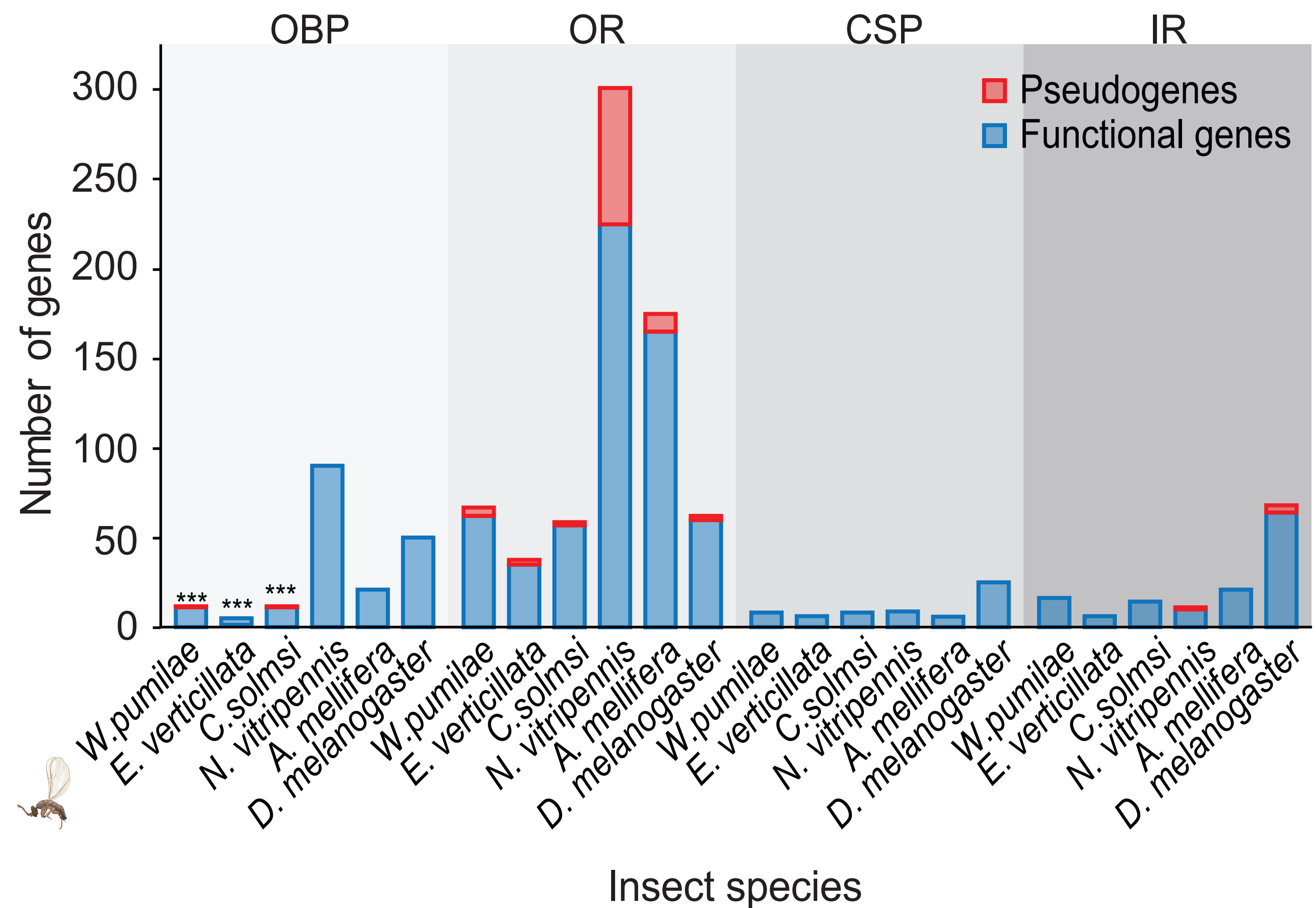
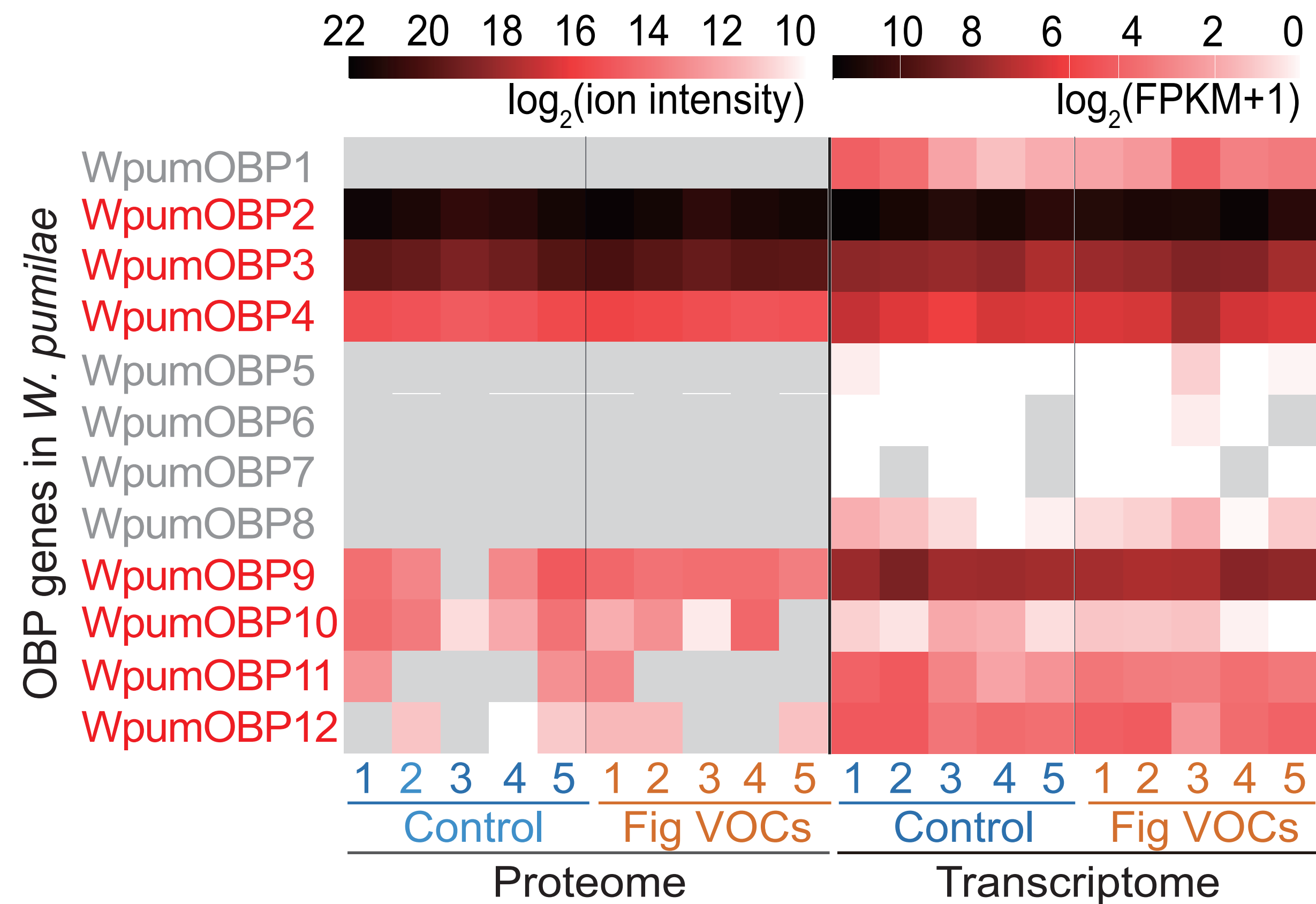
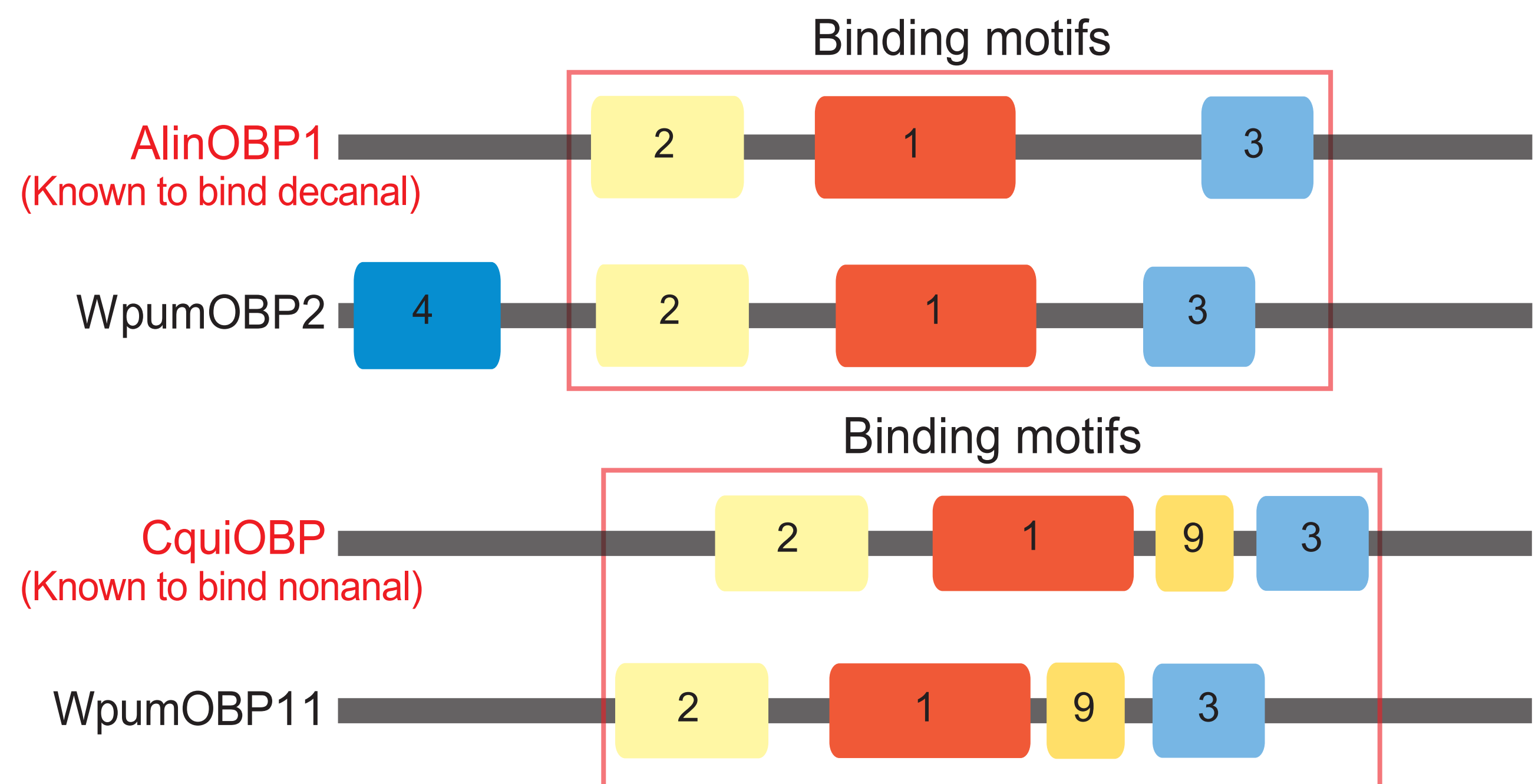
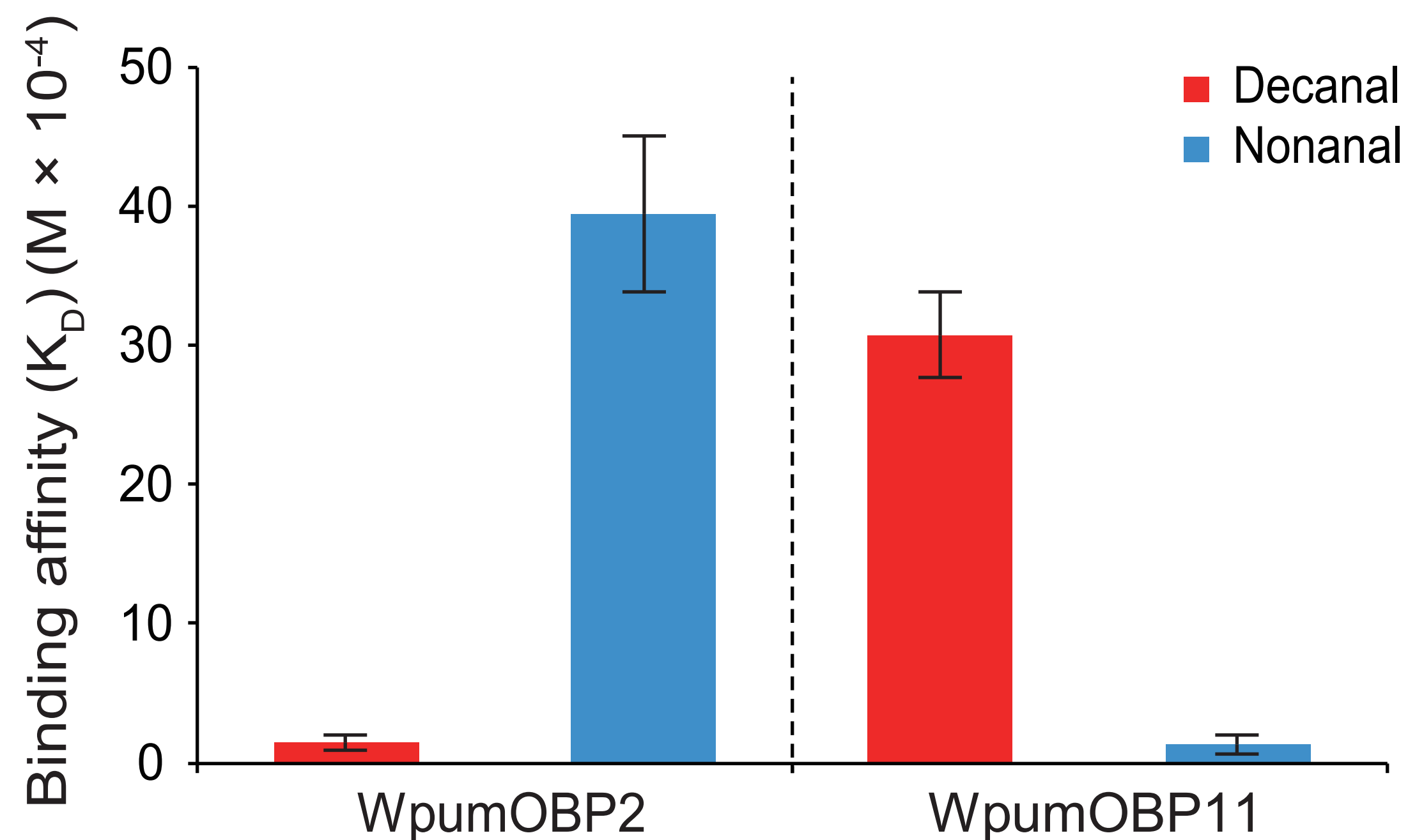
1159 **Code availability**

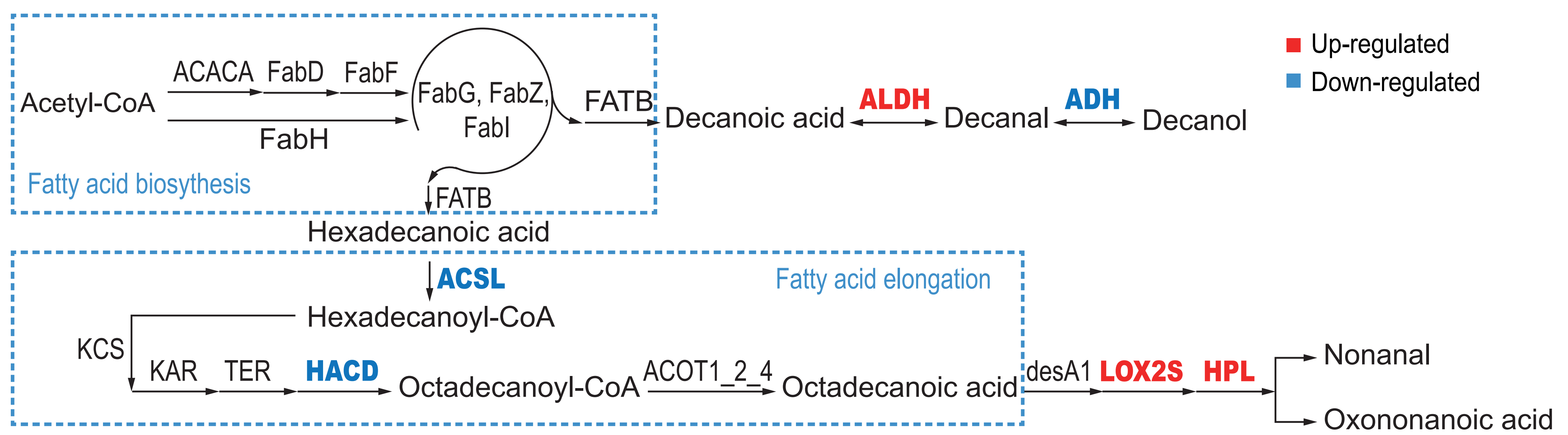
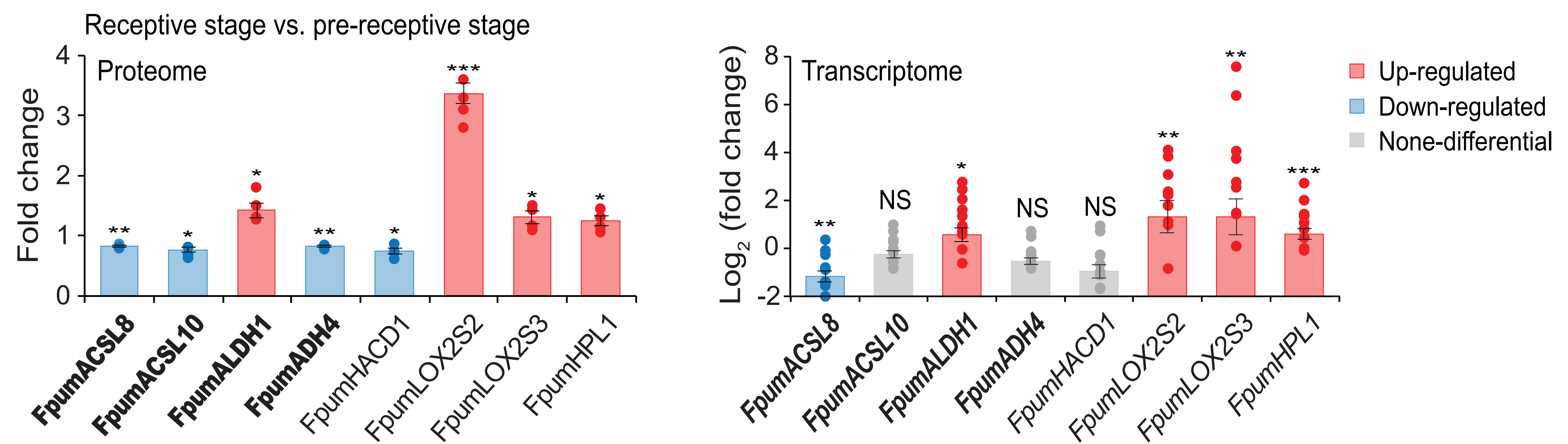
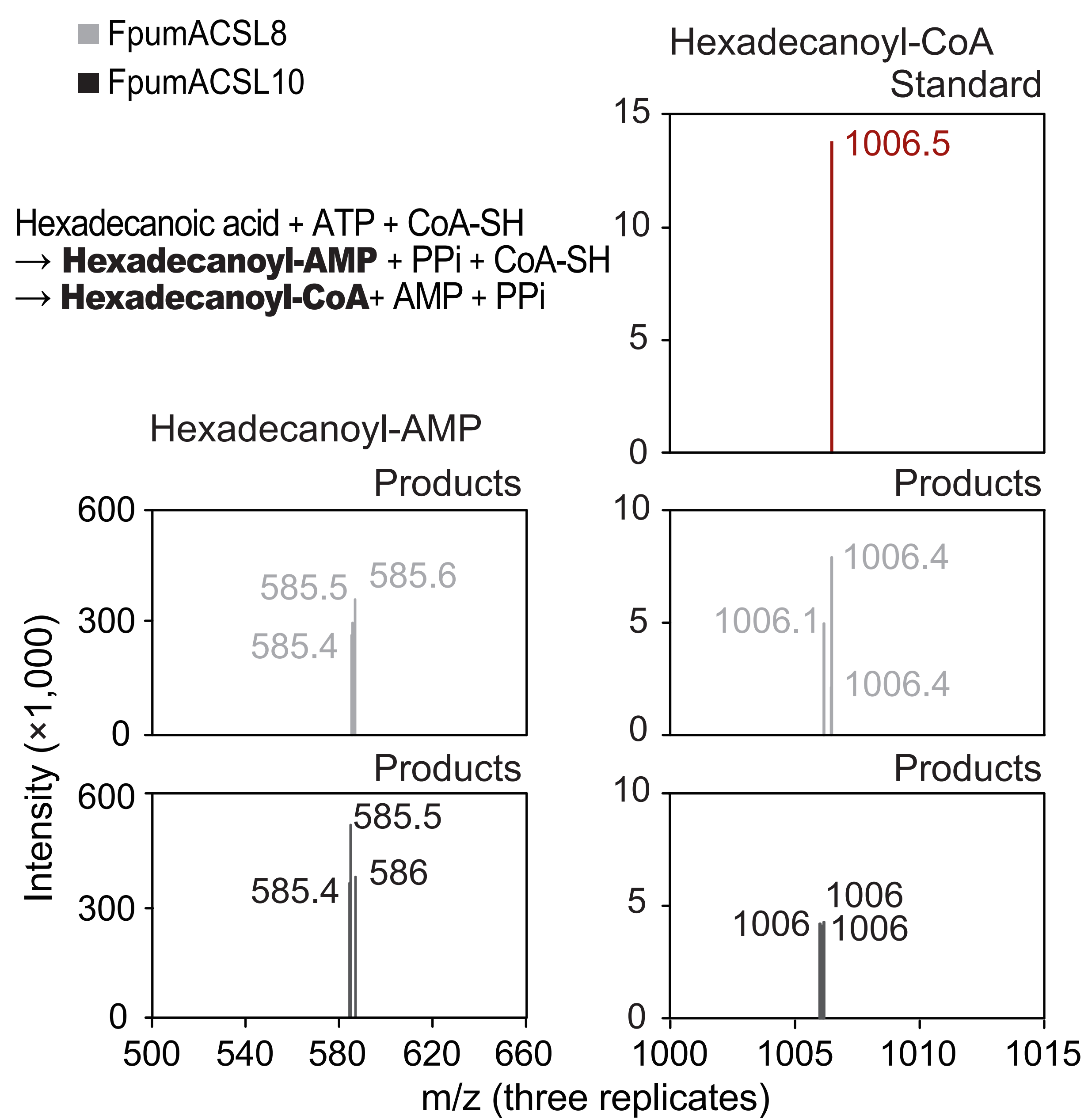
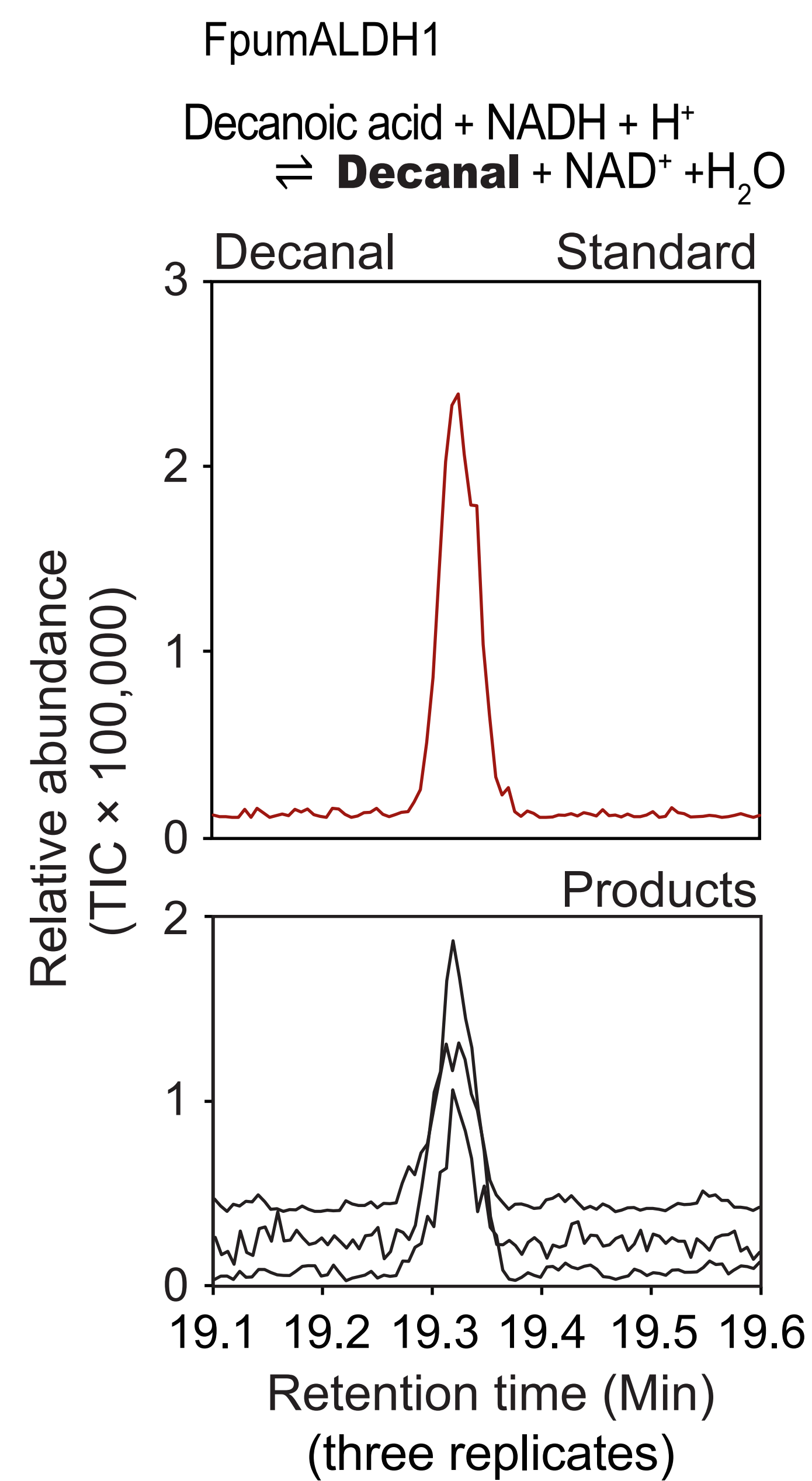
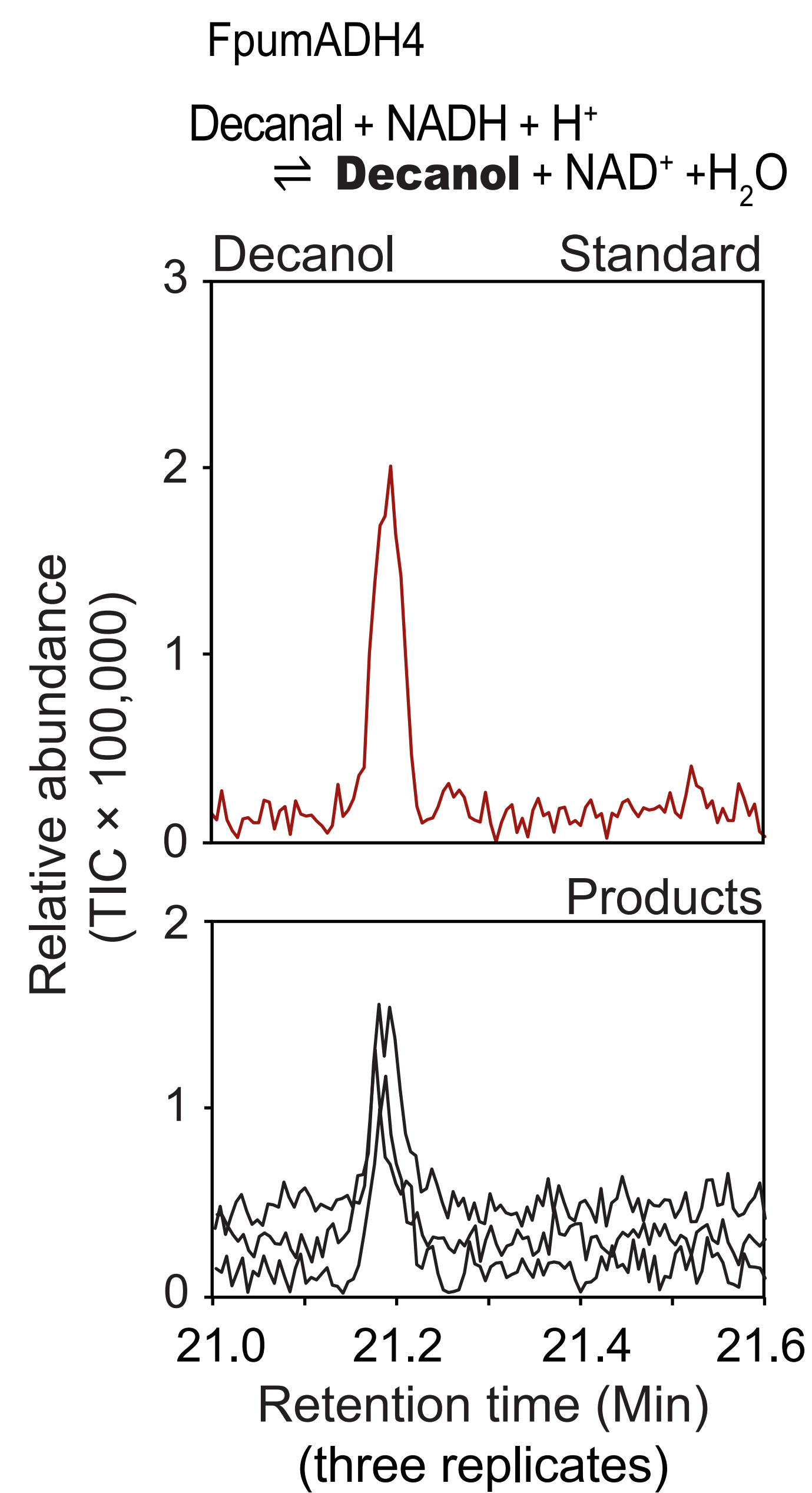
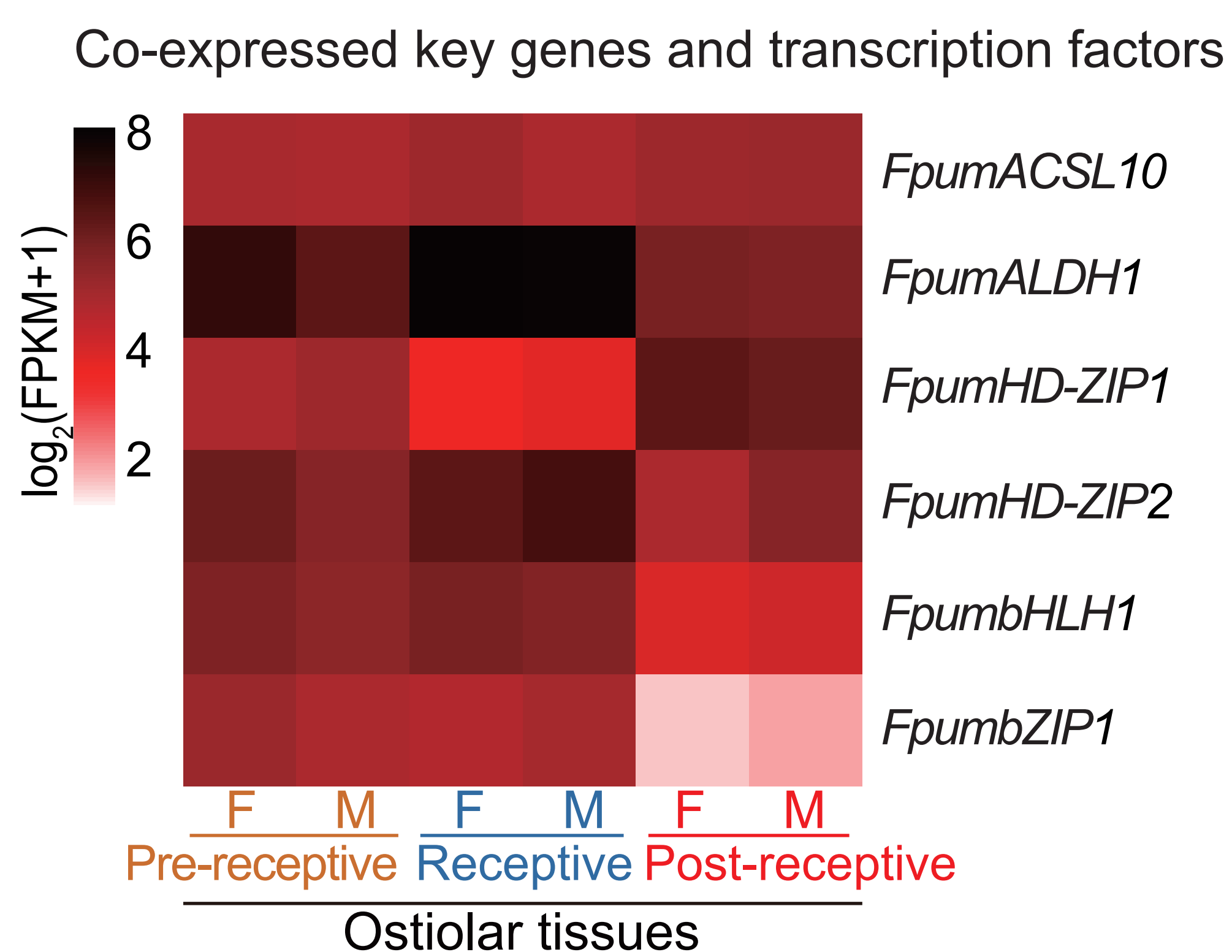
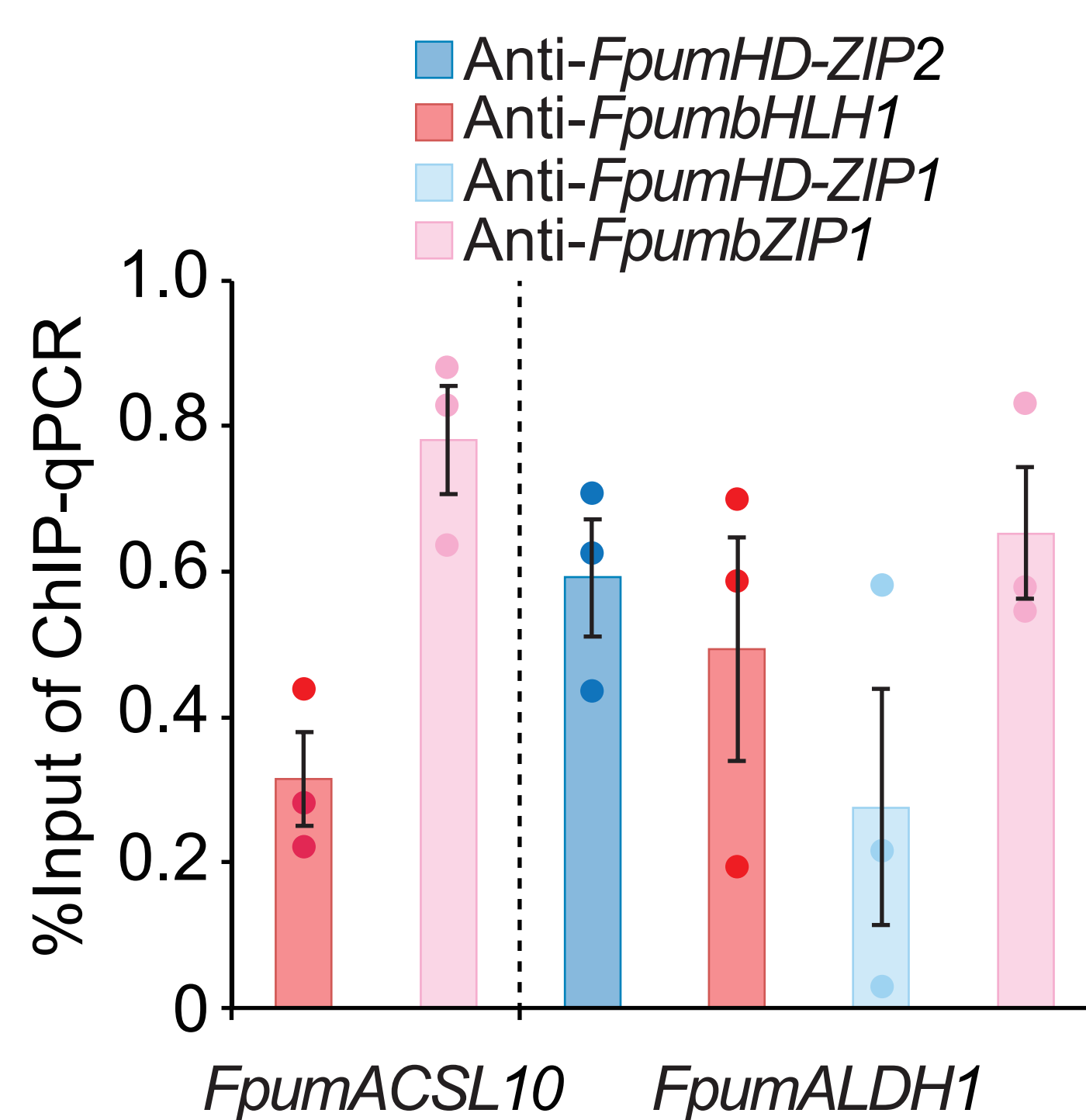
1160 All analyses in this study were conducted using published programs, and all codes for
1161 data analysis are provided in Methods.



a

Olfactory-related gene families

**b****c****d**

a**b****c****d****e****f****g****h**